J Neurophysiol 98: 278–294, 2007.
First published May 9, 2007; doi:10.1152/jn.00306.2007.

Firing Dynamics of Cerebellar Purkinje Cells

Fernando R. Fernandez, Jordan D. T. Engbers, and Ray W. Turner
Hotchkiss Brain Institute, University of Calgary, Calgary, Alberta, Canada

Submitted 19 March 2007; accepted in final form 30 April 2007

Fernandez FR, Engbers JDT, Turner RW. Firing dynamics of cerebellar Purkinje cells. *J Neurophysiol* 98: 278–294, 2007. First published May 9, 2007; doi:10.1152/jn.00306.2007. Knowledge of intrinsic neuronal firing dynamics is a critical first step to establishing an accurate biophysical model of any neuron. In this study we examined cerebellar Purkinje cells to determine the bifurcations likely to underlie firing dynamics within a biophysically realistic and experimentally supported model. We show that Purkinje cell dynamics are consistent with a system undergoing a saddle-node bifurcation of fixed points in the transition from rest to firing and a saddle homoclinic bifurcation from firing to rest. Our analyses account for numerous observed Purkinje cell firing properties that include bistability, plateau potentials, specific aspects of the frequency–current (*F–I*) relationship, first spike latency, and the ability for climbing fiber input to induce state transitions in the bistable regime. We also experimentally confirm new properties predicted from our model and analysis that include the presence of a depolarizing afterpotential (DAP), the ability to fire at low frequencies (<50 Hz) and with a high gain in the *F–I* relationship, and a bistable region limited to low-frequency firing. Purkinje cell dynamics, including bistability, prove to arise from numerous biophysical factors that include the DAP, fast refractory dynamics, and a long membrane time constant. A hyperpolarizing activated cation current (I_H) is shown not to be directly involved in establishing bistable dynamics but rather reduces the range for bistability. A combined electrophysiological and modeling approach thus accounts for several properties of Purkinje cells, providing a firm basis from which to assess Purkinje cell output patterns.

INTRODUCTION

It has become clear that identifying the intrinsic dynamics of neurons is a critical step in the process of understanding network behavior, synaptic integration, and information processing in the brain (Izhikevich 2000, 2007; Izhikevich et al. 2003; Rinzel and Ermentrout 1998). Consequently, gaining a biophysical and dynamical systems perspective of intrinsic neuronal firing behavior is important. From both an electrophysiological and dynamical systems perspective cerebellar Purkinje cells possess complex intrinsic firing behaviors, which include bistability, hysteresis, and plateau potentials (Hounsgaard and Midtgaard 1988; Llinas and Sugimori 1980b; Loewenstein et al. 2005). Given that Purkinje cells integrate numerous synaptic inputs and are the sole output of the cerebellar cortex, an understanding of intrinsic Purkinje cell dynamics is critical to comprehending cerebellar function.

Previous work in vitro has identified numerous intrinsic electrophysiological behaviors of Purkinje cells that are conserved across different species (Hounsgaard and Midtgaard 1988; Llinas and Sugimori 1980a,b; Loewenstein et al. 2005; Williams et al. 2002). Properties that have received particular attention are bistability and the generation of plateau potentials. Recent work has shown that intrinsic membrane bistability allows climbing fiber (CF) input to transition the cell between a rest and firing state (Loewenstein et al. 2005; McKay et al. 2007; Williams et al. 2002). Central to this are plateau potentials that allow an excitatory stimulus to generate a depolarization that outlasts the original stimulus (Llinas and Sugimori 1980a). Other characteristic features of Purkinje cells are a linear frequency–current (*F–I*) relationship with a minimum firing frequency between 40 and 70 Hz and the ability to sustain tonic firing frequencies in excess of 150 Hz (Khaliq et al. 2003; Llinas and Sugimori 1980b; Martina et al. 2003; McKay and Turner 2004, 2005; Williams et al. 2002). Electrophysiological studies have identified many of the ion conductances that contribute to these different aspects of Purkinje cell output (Hounsgaard and Midtgaard 1988; Llinas and Sugimori 1980a,b; Raman and Bean 1999a,b).

Previous modeling studies in Purkinje cells have emphasized how the distribution of ion channels or morphological features of the dendritic tree shape synaptic integration (De Schutter and Bower 1994a,b; Santamaria and Bower 2005; Santamaria et al. 2002) or spike backpropagation (Vetter et al. 2001), or were used to explain a specific property of Purkinje cell firing (Genet and Delord 2002; Khaliq et al. 2003; Loewenstein et al. 2005). We sought a more general firing model based on an understanding from dynamical systems theory that could account for as many properties of Purkinje cells as possible within a realistic biophysical framework. Using a combined electrophysiological, modeling, and dynamical systems analysis we show that Purkinje cell firing dynamics are consistent with a system undergoing a saddle-node bifurcation in the transition from rest to firing and a saddle homoclinic bifurcation from firing to rest [for a review of these concepts and bifurcation theory as applied to intrinsic neuronal biophysics see Izhikevich (2007) or Rinzel and Ermentrout (1998)]. Within this framework we illustrate that numerous aspects of Purkinje cell firing are fundamentally related to the underlying bifurcation structure and further reveal previously unrecognized firing properties of these neurons.

METHODS

Animal care

Sprague–Dawley rats [postnatal day 17 to 25] were obtained from Charles River Laboratories (Quebec, Canada) and procedures were conducted according to guidelines approved by the local Animal Care Committee and the Canadian Council for Animal Care.

Electrophysiology

All chemicals were obtained from Sigma (St. Louis, MO) unless otherwise noted. Whole cell current and voltage-clamp recordings

Address for reprint requests and other correspondence: F. R. Fernandez, Boston University, Biomedical Engineering Department, 44 Cummington St., Boston, MA 02215 E-mail: fernrf@gmail.com).

were obtained using a 700A amplifier (Axon Instruments) and data collected with pCLAMP 8.1 software (Axon Instruments). Tissue slices of cerebellum were prepared as detailed in McKay and Turner (2005). Briefly, artificial cerebrospinal fluid (aCSF) was composed of (in mM): NaCl (125), KCl (3.25), $CaCl_2$ (1.5), $MgCl_2$ (1.5), $NaHCO_3$ (25), and D-glucose (25) preoxygenated by carbogen (95% O_2-5% CO_2) gas. Rats were anesthetized with sodium pentobarbital (MTC Pharmaceuticals, Cambridge, Ontario, Canada). Parasagittal tissue slices (300-μm thickness) were cut and subsequently transferred to the recording chamber of a Zeiss Axioskop FS-2 microscope and maintained at 34°C as a submerged preparation. Neurons were visualized using differential interference contrast optics and infrared light transmission (DIC-IR). All current-clamp recordings were carried out in synaptic blockers that were bath applied after obtaining the initial seal: picrotoxin (50 μM; Tocris Cookson, Ellisville, MO) for γ-aminobutyric acid type A ($GABA_A$) receptors, DL-2-amino-5-phosphonopentanoic acid (D-AP5, 25 μM; Tocris Cookson) for *N*-methyl-D-aspartate receptors, 6,7-dinitroquinoxolinedione (DNQX, 10 μM; Tocris Cookson) for α-amino-3-hydroxy-5-methyl-4-isoxazolepropionic acid receptors, and (2*S*)-3-[[(1*S*)-1-(3,4-dichlorophenyl)-ethyl]amino-2-hydroxypropyl] (phenylmethyl)phosphinic acid (CGP 55845, 1 μM; Tocris Cookson) for $GABA_B$ receptors. Pipettes had a resistance of 5–8 MΩ with access resistance of 6–15 MΩ (80–90% compensation in voltage clamp). The internal solution for current-clamp recordings consisted of (in mM): K-gluconate (130), EGTA (0.1), HEPES (10), NaCl (7), $MgCl_2$ (0.3), di-tris-creatine phosphate (5), Tris-ATP (2), and Na-GTP (0.5) (pH 7.3 with KOH). For outside-out voltage-clamp recordings of K^+ current the internal solution consisted of (in mM): KCl (140), EGTA (5), HEPES (10), and $MgCl_2$ (2.5), with CsCl (2) in the external bath to block the hyperpolarizing activated cation current I_H.

Antidromic stimulations were conducted with a concentric bipolar electrode placed in the white matter region of the folia in the presence of synaptic blockers. Stimuli were delivered by a stimulus isolation unit (DS2 isolation stimulator, Digitimer, Hertfordshire, UK).

Analysis of current-clamp data was accomplished using custom software written in MatLab 7.1 (The MathWorks, Natick, MA). Spike threshold was determined through analysis of the voltage derivative. A calculated junction potential of 11 mV was subtracted from all current-clamp recordings. In voltage-clamp recordings the junction potential was not subtracted because the value was small (~2 mV) for internal KCl.

ZAP protocol

A ZAP protocol consisted of a time-varying current stimulus of 6 s duration generated by the following equations

$$I(t) = \sin[2\pi t f(t)] + I_E$$

$$f(t) = (f_{start} + t f_{rate})/1{,}000$$

$$f_{start} = 0.075 \quad f_{rate} = 0.0075$$

where $I(t)$ is current stimulus, I_E is electrode holding current, and f_{start} and f_{rate} are the initial frequency and rate of change in frequency (in Hz), respectively.

Simulations

Simulations were constructed in MatLab 7.1 using a fourth-order Runge–Kutta algorithm with a time step (dt) of 0.001 ms. Models were formulated using Hodgkin–Huxley formalism. Bifurcation and phase-plane analyses were carried out in XPPAUT v 5.85 (Ermentrout 2002).

Five-equation model

Somatic voltage

$$C_s \frac{dV_s}{dt} = \frac{(V_d - V_s)}{R} + I_E - g_{Na} m_\infty h (V_s - E_{Na^+}) - g_{Ks}(1 - h_s)(V_s - E_{K^+}) - g_{leak}(V_s - E_{leak}) - g_{I_H} ih (V_s - E_{ih})$$

Dendritic voltage

$$C_d \frac{dV_d}{dt} = \frac{(V_s - V_d)}{R} - g_{leak}(V_d - E_{leak}) - g_{Kd(slow)} n_d (V_d - E_{K^+})$$

Na^+ activation

$$m_\infty = \frac{1}{1 + \exp[(V - V_{half})/-k]} \quad V_{half} = -40 \quad k = 3$$

$$\frac{dh}{dt} = \frac{h_\infty - h}{\tau_h} \quad h_\infty = \frac{1}{1 + \exp[(V - V_{half})/-k]} \quad V_{half} = -40 \quad k = -3$$

$$\tau_h(V) = \frac{295.4}{4(V + 50)^2 + 400} + 0.012$$

The h variable represents a merged refractory variable (Na^+ inactivation and K^+ activation).

I_H activation

$$\frac{dih}{dt} = \frac{ih_\infty - ih}{\tau_{ih}} \quad ih_\infty = \frac{1}{1 + \exp[(V - V_{half})/-k]} \quad V_{half} = -80$$

$$k = -3 \quad \tau_{ih} = 100 \text{ ms}$$

Slow K^+ activation

$$\frac{dn_d}{dt} = \frac{n_{d\infty} - n_d}{\tau_{n_d}} \quad n_{d\infty} = \frac{1}{1 + \exp[(V - V_{half})/-k]} \quad V_{half} = -35$$

$$k = 3 \quad \tau_{n_d} = 15 \text{ ms}$$

$C_s = 1.5$ μF/cm^2, $C_d = 1.5$ μF/cm^2, $R = 3/4$, $g_{Na} = 40$ mS/cm^2, $g_{Ks} = 8.75$ mS/cm^2, $g_{I_H} = 0.03$ mS/cm^2, $g_{Kd(slow)} = 12$ mS/cm^2, and $g_{leak} = 0.032$ mS/cm^2.

Testing model robustness

To test for the robustness of the five-equation model individual parameters (maximum conductances, coupling coefficient between compartments, and time constants) were independently varied by as much as 20% from the default values. Under all cases the model retained the key characteristics described in this study provided that the bias current (I_E) was adjusted to compensate for small changes in threshold. Properties tested include a substantial bistable range (>0.15 μA/cm^2), the ability to generate a long delay to first spike relative to the subsequent ISI, the generation of a DAP, and the ability for a unipolar input to switch between a rest and firing state.

Reduced two-equation model

$$C \frac{dV}{dt} = I_E - g_{Na} m_\infty (1 - n)(V - E_{Na^+}) - g_K n (V - E_{K^+}) - g_{leak}(V - E_{leak})$$

Na^+ activation

$$m_\infty = \frac{1}{1 + \exp[(V - V_{half})/-k]} \quad V_{half} = -35 \quad k = 5$$

K^+ activation

$$\frac{dn}{dt} = \frac{n_\infty - n}{\tau_n} \quad n_\infty = \frac{1}{1 + \exp[(V - V_{half})/-k]} \quad V_{half} = -36$$

$$k = 5 \quad \tau_n = 0.6 \text{ ms}$$

$C = 1.5\ \mu F/cm^2$, $g_{Na} = 20\ mS/cm^2$, $g_K = 4.2\ mS/cm^2$, and $g_{leak} = 0.05\ mS/cm^2$.

For all simulations reversal values were set to: $E_{Na^+} = 45$ mV, $E_{K^+} = -95$ mV, $E_{I_H} = -20$ mV, and $E_{leak} = -77$ mV.

RESULTS

Threshold dynamics in Purkinje cells are consistent with a saddle-node bifurcation of fixed points

Understanding the dynamics governing the transition from rest to firing is critical because it will largely set the dynamical framework from which many properties of Purkinje cell firing may be accounted for. We started by considering the type of bifurcation underlying Purkinje cell spike threshold. In brief, a bifurcation can often consist of a qualitative change in the system dynamics (e.g., transition from rest to firing) that involves the creation or elimination of fixed points or limit cycles. A neuronal resting state is an example of a stable fixed point and a spiking state a limit cycle (Izhikevich 2000, 2007; Rinzel and Ermentrout 1998; Strogatz 1994). The type of bifurcation that the Purkinje cell undergoes at threshold will largely determine the potential nature of a plateau potential and bistability (Izhikevich 2000, 2007; Rinzel and Ermentrout 1998).

The two principal types of bifurcation governing thresholds in neurons are a Hopf bifurcation and a saddle-node bifurcation (Izhikevich 2000, 2007; Rinzel and Ermentrout 1998). An important criteria for identifying the type of bifurcation underlying spike threshold are steady-state current–voltage (*I–V*) relationship and the voltage trajectory in the subthreshold range (Izhikevich 2000, 2007; Rinzel and Ermentrout 1998). These two factors can be used to differentiate whether a cell undergoes a saddle-node bifurcation of fixed points or a Hopf bifurcation when driving current is the sole bifurcation parameter. In essence, the presence of a highly nonlinear *I–V* relationship with an abrupt increase in membrane voltage deflections (resistance) near threshold is consistent with a saddle-node bifurcation. The ability to generate long delays to first spike is also consistent with a saddle-node bifurcation. Finally, an approach to spike threshold with no fast subthreshold or damped oscillations in membrane voltage, combined with long first delays to the first spike, are also consistent with a saddle-node bifurcation (Izhikevich 2000, 2007). Thus we evaluated the *I–V* relationship and subthreshold voltage trajectory to distinguish which bifurcation was consistent with the activity of Purkinje cells.

To evaluate the steady-state *I–V* relationship the membrane potential was held near −71 mV and stepped to voltages ranging from −74 to −64 mV in 10 pA increments for 350 ms. Membrane voltage was measured at 275 ms, which provided sufficient time for the I_H-mediated sag in the voltage response to equilibrate. As previously shown (Llinas and Sugimori 1980a,b), Purkinje cells showed a highly nonlinear *I–V* relationship for depolarizations greater than −70 mV (Fig. 1, *A* and *B*). Application of TTX resulted in a linear *I–V* relationship, indicating a steady-state activation of Na^+ current that increased the slope of the *I–V* relationship and thus the input resistance in this voltage region (Fig. 1, *A* and *B*). This occurs because a steady-state negative conductance acts to increase the amplitude of positive and negative voltage deflections by increasing the inward current with depolarization (amplifying a depolarization) and decreasing inward current with hyperpolarization (amplifying a hyperpolarization) (Stafstrom et al. 1982). From a

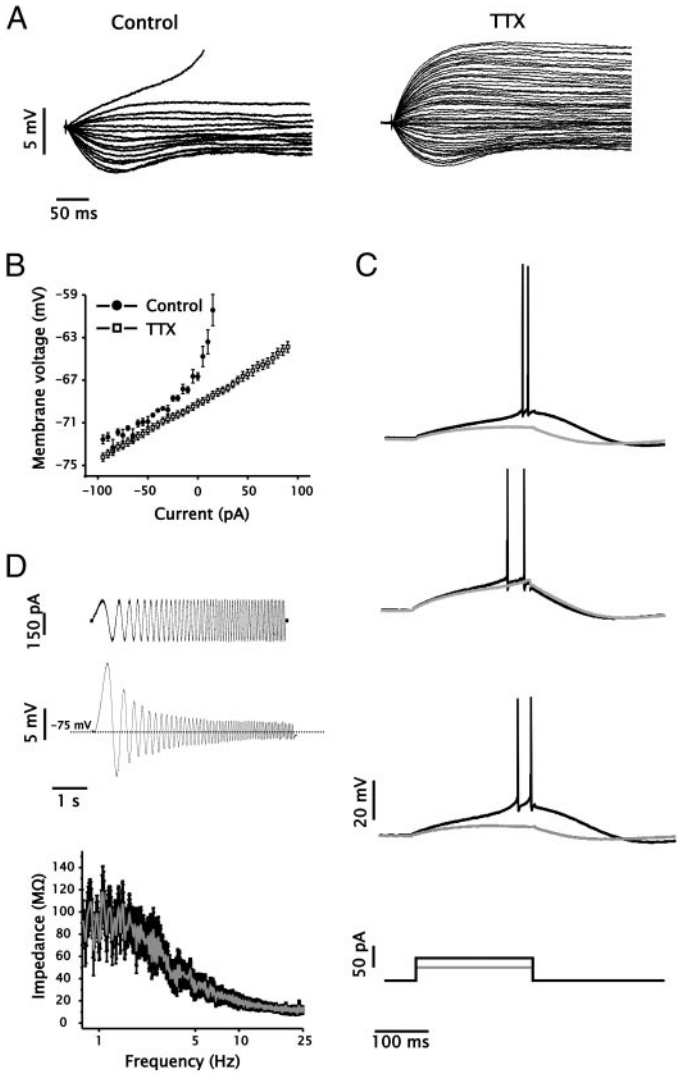

FIG. 1. Threshold dynamics of Purkinje cells. *A*: representative membrane voltage traces with or without 100 μM bath-applied tetrodotoxin (TTX) in response to 350 ms square-wave current steps ranging from −100 to 100 pA. Membrane potential was held at approximately −71 mV. *B*: steady-state current–voltage (*I–V*) relationship with or without TTX ($n = 6$). Membrane voltage was measured 275 ms after the onset of the current step. *C*: representative voltage trajectory for 3 different Purkinje cells with subthreshold (gray) or suprathreshold (black) stimulation intensity. Membrane potential was held at −70 mV and stepped depolarized with <50 pA of driving current. Note that Purkinje cells are able to generate long first spike latency times. *D*: subthreshold membrane impedance profile determined using a ZAP protocol. Membrane potential was initially held at −75 mV and driven with a ZAP current protocol of 6 s duration with a slowly increasing frequency. In the *bottom plot* of impedance measurements, the gray line denotes average impedance ($n = 8$), whereas SE bars are denoted with black lines. Impedance was calculated as the ratio of the Fourier transform between the subthreshold voltage response and the applied current.

dynamical systems perspective the rapid increase in membrane input resistance can represent a nonmonotonic relationship in the steady-state *I–V* relationship. This nonmonotonicity is critical for producing the fold associated with the coalescing of a node and saddle point, and thus a saddle-node bifurcation (Izhikevich 2000, 2007; Rinzel and Ermentrout 1998). Purkinje cells thus satisfy the criterion of exhibiting a nonlinear steady-state *I–V* relationship with a dramatic increase in input resistance near threshold necessary for a saddle-node bifurcation of fixed points.

We next tested whether Purkinje cells could generate long first spike latency times. To accomplish this we held Purkinje cells at −70 mV and provided a weak depolarizing input (usually <50 pA). Under these conditions all Purkinje cells tested could generate first spike latencies in excess of 150 ms (Fig. 1*C*). Furthermore, in the subthreshold voltage trajectory leading up to the first spike there was a clear absence of damped or sustained fast oscillatory activity, as predicted for a saddle-node bifurcation. Note that although the initial first spike latency was long, the subsequent interspike intervals (ISIs) were always shorter than the initial spike delay. Although this trajectory is often attributed to a subthreshold inactivating K^+ current (I_A), we and others find no evidence for this current in outside-out patches obtained from mature Purkinje cells (Supplementary Fig. 1)[1] (Martina et al. 2003; McKay and Turner 2004). Previous work in mouse Purkinje cells has shown evidence for a subthreshold inactivating K^+ current (Sacco and Tempia 2002). These experiments, however, were carried out in postnatal day 3 to 9 animals. Their results are thus consistent with immunohistochemical data that indicate only a transient early developmental expression of channels contributing to the A-type current (Hsu et al. 2003). Thus our data support previous conclusions that A-type currents are absent in mature rat Purkinje cells.

As a final test for the type of bifurcation governing threshold dynamics in Purkinje cells we applied a ZAP protocol. A ZAP protocol provides a simple method to assess the subthreshold impedance of neurons by stimulating the neuron with sinusoidal current with a slowly increasing frequency (Hutcheon and Yarom 2000). Neurons that undergo a Hopf bifurcation have a dampening conductance active below threshold that acts similar to an inductor (Izhikevich 2007). Consequently, when combined with the membrane resistance and capacitance, neurons undergoing a Hopf bifurcation resonate at intermediate frequencies of subthreshold stimulation, which produces a band-pass impedance profile. Conversely, neurons undergoing a saddle-node bifurcation have no resonance behavior and thus have a low-pass impedance profile associated with the membrane resistance and capacitance (Izhikevich 2007). As shown in Fig. 1*D*, application of a ZAP protocol produced no resonance behavior in the Purkinje cell membrane voltage response and also produced a monotonic membrane impedance profile ($n = 8$).

In summary, these simple experiments provide evidence that Purkinje cell spike threshold dynamics are consistent with a saddle-node bifurcation of fixed points. They also confirm that a steady-state Na^+ current is the principal determinant of the nonlinearities in the subthreshold range of the *I–V* curve. Thus as the membrane voltage approaches threshold, more net inward current with a negative conductance is activated. Consequently, from a dynamical systems perspective any model of Purkinje cell firing and bistability must incorporate a saddle-node bifurcation of fixed points to account for the physiological properties apparent during the transition from rest to firing.

Purkinje cells respond nonmonotonically to climbing fiber–like stimuli

Previous work has established that Purkinje cells have the ability to switch from rest to firing as well as from firing to rest in response to a strong unipolar current input (Fig. 2*A*) (Loewenstein et al. 2005). Consequently, bistability in Purkinje cells occurs between a fixed point and a limit cycle. This differs from some neurons that have been shown to be bistable in which the two stable states are represented by a hyperpolarized or depolarized resting state (Crunelli et al. 2005; Williams et al. 1997). Physiologically such a unipolar input can be provided by climbing fiber (CF) activation, which induces a strong synaptic current lasting about 15 ms (Schmolesky et al. 2002). Therefore in the next set of experiments we focused on the intrinsic dynamics of Purkinje cell firing in the context of postsynaptic CF-like stimuli. In particular, we were interested in whether the membrane voltage response of Purkinje cells to CF-like stimuli could further constrain our identification of dynamics underlying spike firing (Fig. 1).

We regarded the large complex spike depolarization triggered by CF input as a strong perturbation comparable to changing the initial conditions of a model. To facilitate analysis of Purkinje cell dynamics and modeling we used square intracellular current steps of varying amplitude and fixed duration (0.25 to >5 nA; 15 ms) to simulate the depolarization associated with a complex spike. For these experiments Purkinje cells were held at −68 mV with approximately −50 pA. As shown in Fig. 2*B*, the ability to switch from rest to firing depended on the amplitude of the stimulus. As expected, weak stimulation (0.25 nA) had a very low probability of inducing a state transition to firing (0.22 ± 0.10; $n = 5$), although it could produce a prolonged (100 ms) subthreshold plateau depolarization after the end of the current step (Fig. 2*C*). We also found that very strong stimulations (>5 nA) were relatively unsuccessful in inducing transitions to the firing state (0.04 ± 0.04; $n = 5$). In these cases membrane voltage rapidly returned to rest after stimulation and was often followed by a transient hyperpolarization. Intermediate-size stimuli (0.5–2 nA) were the most successful in inducing a transition from the rest to firing state (Fig. 2*C*; 0.96 ± 0.04; $n = 5$).

A simple explanation for the nonmonotonicity in the relationship between CF-like stimulus magnitude and state transition probability is that stronger stimulation recruits a greater amount of K^+ current activation or Na^+ current inactivation. This in turn brings about a failure to transition to the firing state and a rapid return to the rest state. In fact, this can be observed in the rate of repolarization after different magnitudes of CF-like stimuli. To test this we held cells at a slightly more negative membrane potential (−74 mV) so that the cell did not transition to the firing state and the rate of repolarization after stimulation could be observed. We used three different strengths of CF-like stimuli (1, 2, and 5 nA). As expected, the membrane potential returned more quickly to baseline voltage

[1] The online version of this article contains supplemental data.

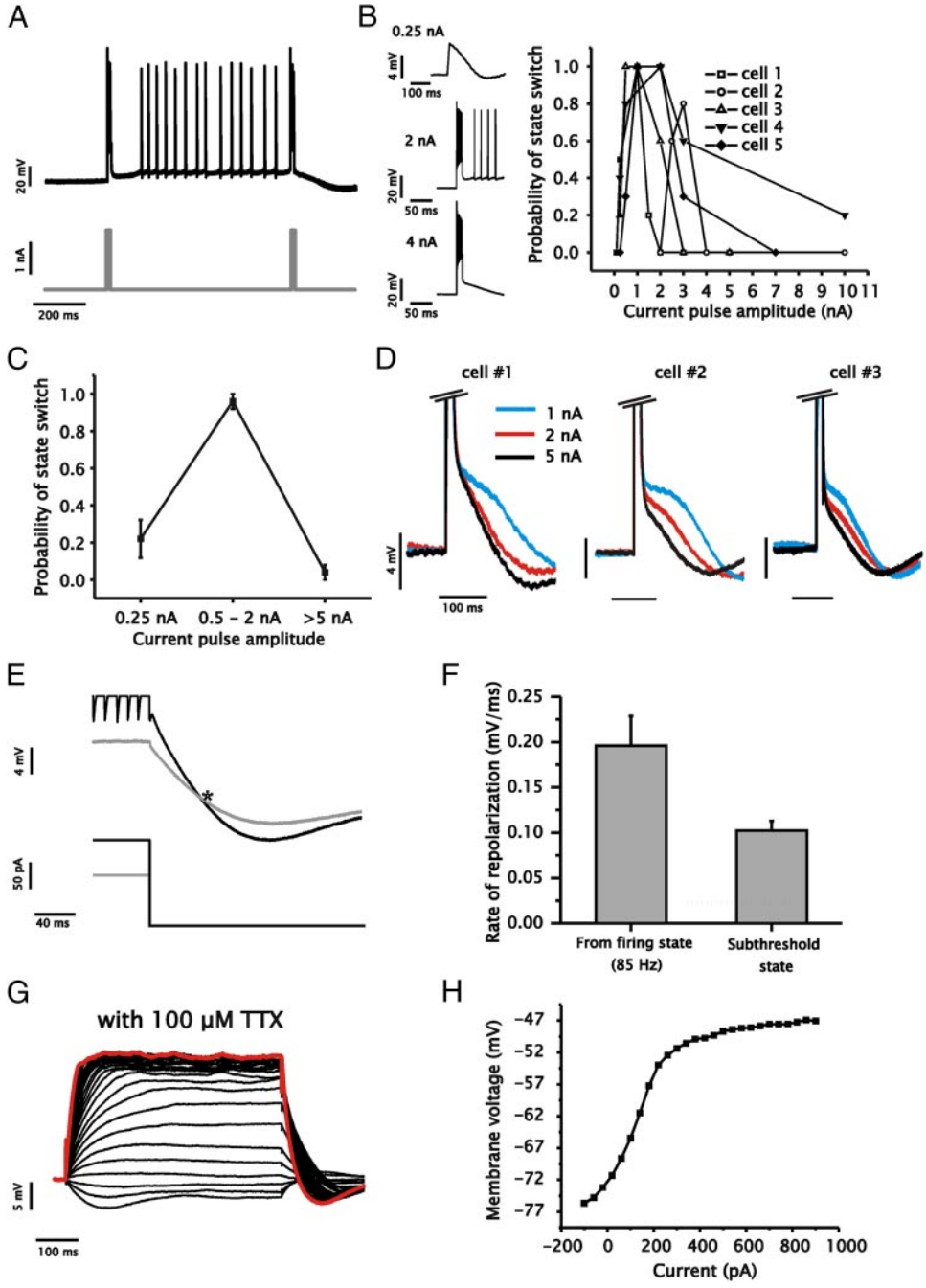

FIG. 2. Dynamics of Purkinje cell bistability in response to climbing fiber (CF)–like stimuli. *A*: representative voltage trace of a Purkinje cell in response to 2 consecutive CF-like stimuli [2-nA, 15-ms, 600-ms interspike interval (ISI)] from a membrane potential of −69 mV showing the toggling of spike output between rest and firing. *B*: membrane response to CF-like stimuli of different magnitudes. Cells were held at about −68 mV and given a CF-like stimulus ranging from 0.25 to 10 nA. Representative membrane voltage response to CF-like stimuli of 0.25, 2, and 4 nA (15 ms) (*left*). Plot of the probability of evoking a state transition from rest to firing for 5 separate cells (*right*) determined using 10 stimulations at the indicated CF-like stimulus amplitude. *C*: plot of the averaged binned response for data shown in *B*. Note that CF-like stimuli of 0.5–2 nA significantly increase the probability of obtaining a state transition compared with amplitudes <0.25 and >5 nA ($P < 0.01$, $n = 5$). *D*: superimposed representative voltage traces for 3 separate cells in response to CF-like stimuli of different pulse amplitude (15 ms). Initial membrane potentials were −75 mV. *E*: 2 expanded and superimposed voltage traces illustrating the rate of repolarization immediately after sub- and suprathreshold square-wave current steps. Cells were initially held at −75 mV and step depolarized for 200 ms using either 100 pA (subthreshold; *gray trace*) or 175 pA (suprathreshold; *black trace*). Spikes in the *top trace* have been truncated. Rate of repolarization was measured from the point of stimulus cessation to the point when membrane voltage traces were first equal in value (asterisk). *F*: plots of the average rate of repolarization after cessation of sub- and suprathreshold current steps as shown in *E* ($P < 0.01$, $n = 5$). *G*: representative voltage response in a Purkinje cell to 500-ms step depolarizations from −100 to −900 pA in 50-pA increments in the presence of 100 μM TTX. Largest depolarization (*red trace*, peak voltage of −47 mV) was the fastest to repolarize. Cell was initially held at about −71 mV. *H*: steady-state *I–V* relationship in the presence of 100 μM TTX measured 275 ms after onset of the current step, as shown in *H*. Note that the *I–V* relationship begins to saturate at voltages above −52 mV.

after stronger stimulation (Fig. 2*D*), which suggested the recruitment of a K^+ current or inactivation of Na^+ current.

An interesting aspect of Purkinje cell state transitions is that the same magnitude depolarizing pulse can induce transitions both from rest to firing and from firing back to rest (Fig. 2*A*) (Loewenstein et al. 2005). The ability for such a unipolar and fixed input (i.e., complex spike depolarization) to toggle the cell between firing and rest states may also be accounted for in terms of the relative activation of K^+ and Na^+ currents. Thus the firing state recruits more net K^+ current or Na^+ inactivation than at rest, allowing a CF-like stimulus to switch the cell to the rest state. If this scenario is valid it would be expected that the rate of repolarization after a square-step depolarization that induced a moderate rate of firing would be greater than a similar step that is slightly subthreshold because, during the firing state, more K^+ current activation or Na^+ inactivation would be present. Once again we held cells at a sufficiently negative membrane voltage to avoid state transitions and observed the rate of repolarization after the step pulse. We used a 200 ms step depolarization of either 100 pA (subthreshold) or 175 pA (suprathreshold and firing at ~80 Hz) from a holding potential of −75 mV. As shown in Fig. 2, *E* and *F*, the rate of repolarization after a step depolarization was faster if the cell membrane potential returned to baseline from a firing state rather than a depolarized but subthreshold state.

Because of the absence of spiking in the presence of TTX we could measure the *I–V* relationship over a wider range of membrane voltages. In particular, we were interested in the

conductance behavior at increasingly depolarized membrane voltages. We reasoned that if increasing depolarization induces a faster rate of repolarization to the rest state, then the *I–V* relationship should indicate a strong saturation (decrease in input resistance) at more depolarized membrane potentials. Furthermore, if the rate of repolarization in the presence of TTX is greater when preceded by a stronger depolarization it indicates that depolarization activates a K^+ conductance that facilitates repolarization on cessation of the current step. This prediction was borne out in the steady-state *I–V* relationship of Purkinje cells, which began to saturate at membrane voltages greater than −50 mV in the presence of TTX (Fig. 2, *G* and *H*). This was also accompanied by an increase in the rate of repolarization after cessation of stronger depolarizing steps (Fig. 2*G*). These results are consistent with an increased activation of K^+ current during the firing state that deactivates slowly enough to influence the rate of repolarization at the end of the current step. Thus the same depolarizing stimulus that switched a cell to the firing state can be used to switch the cell back to the rest state through the additional activation of K^+ current.

A model of Purkinje cells indicates the dynamical basis of bistability

To gain greater insight into Purkinje cell firing dynamics we constructed a firing model. We used the data on threshold dynamics, which indicated the presence of a saddle-node bifurcation, and the membrane voltage response to CF-like stimuli as a general framework for the model's dynamics and biophysics. We also considered experimental results from previous electrophysiological studies of Purkinje cells. We started by incorporating the essential elements required to reproduce basic properties of Purkinje cell behavior, including a somatic and dendritic compartment and conductances required to generate spike firing.

Previous work has shown that a portion of Purkinje cells can produce a three-stage trimodal firing pattern that arises when cells fire at sufficiently high frequencies (McKay and Turner 2004; Womack and Khodakhah 2002). In our experiments we found that approximately half of Purkinje cells at the age examined could develop a trimodal firing pattern. Recent in vitro work, however, reveals that reintroducing low-frequency (~1 Hz) CF activation or strong depolarization inhibits trimodal firing and stabilizes Na^+ spike output at a new lower-frequency level (McKay et al. 2007), whereas the removal of CF inputs in vivo leads to trimodal-like activity (Cerminara and Rawson 2004). This suggests that the tonic firing behavior is most likely the normal firing mode for Purkinje cells in vivo. For these reasons we did not incorporate trimodal firing dynamics in our model.

We first considered the addition of a dendritic compartment given the important role this can have in establishing spike firing behavior (Doiron et al. 2001; Fernandez et al. 2005; Mainen and Sejnowski 1996). It has been established that Purkinje cell dendrites do not generate active regenerative events (Na^+ or Ca^{2+} spikes) during tonic repetitive Na^+ spiking at the soma (McKay and Turner 2004; Stuart and Hausser 1994). Consequently, the charging of the dendritic compartment draws current away from the active zone in the soma/axon hillock, raising current threshold at the active zone. Once charged, however, the relative absence of fast voltage-gated Na^+ and K^+ conductances in dendrites prevents the dendritic membrane voltage from equilibrating at the same time as the somatic compartment. This causes the dendritic membrane potential to remain positive relative to the somatic compartment for a substantial period of time during an ISI. This behavior is in fact consistent with dual-patch recordings from Purkinje cell soma and dendrite, where dendritic membrane voltage remains at a more depolarized level during the somatic afterhyperpolarization (AHP) (McKay and Turner 2004; Stuart and Hausser 1994). This property has also been recognized as important in previous models of Purkinje cells (Jaeger et al. 1997). To simplify the model as well as facilitate analysis we used a reduction approach developed by Pinsky and Rinzel (1994). With this reduction the two compartments influence each other through a current term that is proportional to the difference in voltage between the two compartments and scaled by a term representing the resistance between the compartments (Pinsky and Rinzel 1994). In our model we used a coupling resistance between the two compartments that reproduced the delay and voltage drop observed in dual soma-dendritic recordings (see METHODS) (McKay and Turner 2004; Stuart and Hausser 1994).

The somatic compartment contains a transient Na^+ current and a noninactivating K^+ current. The dendritic compartment contains a slow K^+ current subsequently described. To reduce the dimensionality of the model we set Na^+ activation to equilibrate instantaneously with voltage and described Na^+ inactivation and K^+ activation as h and $1 - h$, respectively (Rinzel 1985). Furthermore, to take into account the fast refractory dynamics observed in Purkinje cells, we made the time constant of the refractory variable (h) relatively fast (0.1–0.9 ms) to permit the model to fire at frequencies >150 Hz. This is consistent with previous work in Purkinje cells that established that fast activating and deactivating K^+ currents as well as a resurgent Na^+ current enable high-frequency firing by contributing to a greater net depolarization between spikes (Khaliq et al. 2003; Martina et al. 2003; McKay and Turner 2004; Raman and Bean 1999a,b, 2001; Swensen and Bean 2003). More recent work has shown that Purkinje cells express exceptionally fast K^+ currents with activation and deactivation time constants ranging from 0.2 to 2.5 ms when measured at room temperature (Martina et al. 2007). Finally, we selected a leak conductance density that produced an approximate membrane time constant of 90 ms, which is within the range measured in previous studies (Rapp et al. 1994; Roth and Hausser 2001).

The TTX-sensitive Na^+ current that contributes to a nonlinear increase in membrane voltage at depolarized potentials (Fig. 1*B*) may arise through a steady-state Na^+ window current or a persistent (noninactivating) Na^+ current (Stafstrom et al. 1982). To incorporate this in the model we set Na^+ conductance to have a window current by providing an overlap in the steady-state activation and inactivation variables. The model also includes a greater Na^+ current density relative to K^+ and leak current. In doing so we ensure that more net Na^+ current activates at subthreshold membrane voltages (−70 to −65 mV) than K^+ or leak current, which reproduces the nonlinearity in voltage response in the subthreshold region (Fig. 3*B*). A persistent Na^+ current is not included because the Na^+ window current is sufficient to reproduce the experimentally observed *I–V* relationship. In Fig. 3*A* we have calculated the steady-state *I–V* relationship as a function of membrane voltage for the entire model—both the total current and each

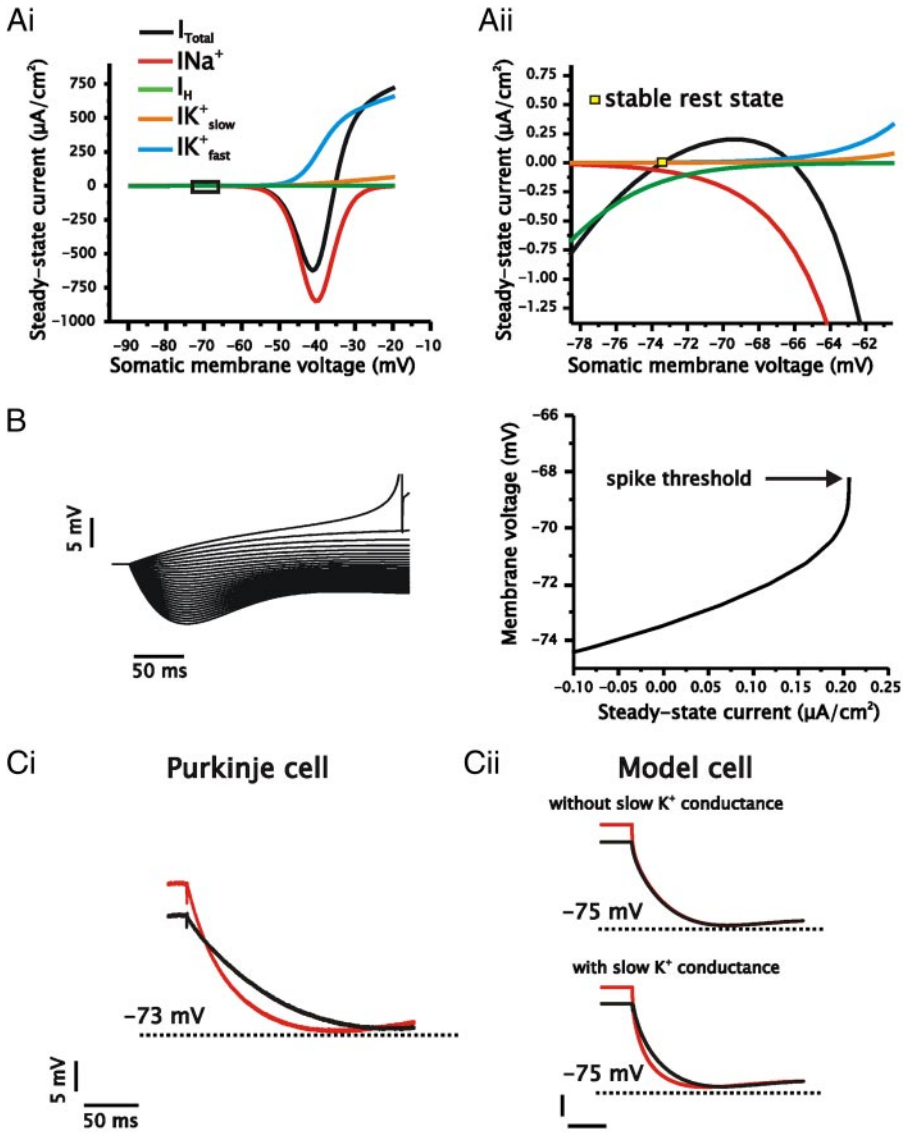

FIG. 3. Construction of a firing model based on the *I–V* relationship of Purkinje cells. *A*: steady-state *I–V* relationship for active conductances in the firing model. Area around spike threshold (*Aii*, boxed area in *Ai*) is nonmonotonic as a result of substantial activation of Na^+ conductance near spike threshold. Note that the intersection of the total steady-state *I–V* relationship (black line) with the zero current line when the total steady-state *I–V* has a positive slope corresponds to the stable rest state of the model neuron. *B*: voltage response and steady-state *I–V* relationship of the model in response to square-wave current steps (measured 275 ms after pulse onset). Model was initially held at −72 mV and stepped from −74.5 to −68 mV, with current steps ranging from −0.1 to 0.2 $\mu A/cm^2$. *C*: comparison of the rate of repolarization after strong depolarization in the Purkinje cell (*Ci*) and model cell (*Cii*) in the absence of Na^+ conductance. For the cell Na^+ conductance was removed with 100 μM TTX, whereas in the model $g_{Na_{max}}$ was set to 0 mS/cm^2. Purkinje cell (*Ci*) and model (*Cii*) were depolarized to −50 mV (red line) or −55 mV (black line) for 500 ms using a square-wave current step. In the cell the membrane voltage repolarizes faster from a depolarized state. Reproducing this in the model requires the presence of a slow K^+ conductance (*Cii*). Cell and model were initially held at −73 and −75 mV, respectively.

individual active conductance. As expected, the steady-state *I–V* relationship for the total current is nonmonotonic with a fold region corresponding to the increase in input resistance during the approach to threshold (Fig. 3*A*). Consequently, the steady-state *I–V* relationship for the model as a function of *current* is nonlinear with increasing input resistance at depolarized membrane potentials similar to that observed in Purkinje cells (cf. Figs. 1*B* and 3*B*).

The time course of the membrane voltage response of Purkinje cells to step depolarizations in the presence or absence of TTX suggested the expression of an additional slower K^+ current (Fig. 1*A*). Greater depolarization was also associated with a faster rate of repolarization on cessation of a depolarizing current step (Fig. 2, *E* and *G*). Although the fast K^+ current in the model can account for the saturation in the steady-state *I–V* plot in the presence of TTX, it cannot reproduce the faster repolarization after strong depolarization (Fig. 3*C*). In essence, the short time constant for the fast K^+ current causes it to turn off too quickly to influence the time course of repolarization. To reproduce this behavior in the model requires the addition of a slower K^+ current with a time constant of 15 ms (Fig. 3*Cii*). This slow K^+ conductance could arise from an interaction between internal Ca^{2+} and Ca^{2+}-activated K^+ channels (Hounsgaard and Midtgaard 1989). However, we did not model Ca^{2+}-dependent K^+ currents explicitly because of the increase in dimensionality this approach requires and the lack of experimental data on the specific biophysics governing intracellular Ca^{2+} dynamics in Purkinje cells. This does not affect the fundamental formulation of the model because, from a dynamical systems perspective, it is not critical whether the K^+ conductances are voltage-gated indirectly through voltage-gated Ca^{2+} channels or directly through an intrinsic voltage sensor. Finally, we incorporated I_H into the model using parameters established by previous experimental studies (Roth and Hausser 2001; Williams et al. 2002), which reproduced the typical sag in the membrane voltage associated with hyperpolarization (Fig. 3*B*).

To establish the performance of our model to Purkinje cells we began by comparing the responses evoked by step depolarizations of 250 ms. Purkinje cells were held at −74 mV and depolarized with a maximum of 200 pA (Fig. 4*Ai*). In comparison, our model is able to reproduce the major characteris-

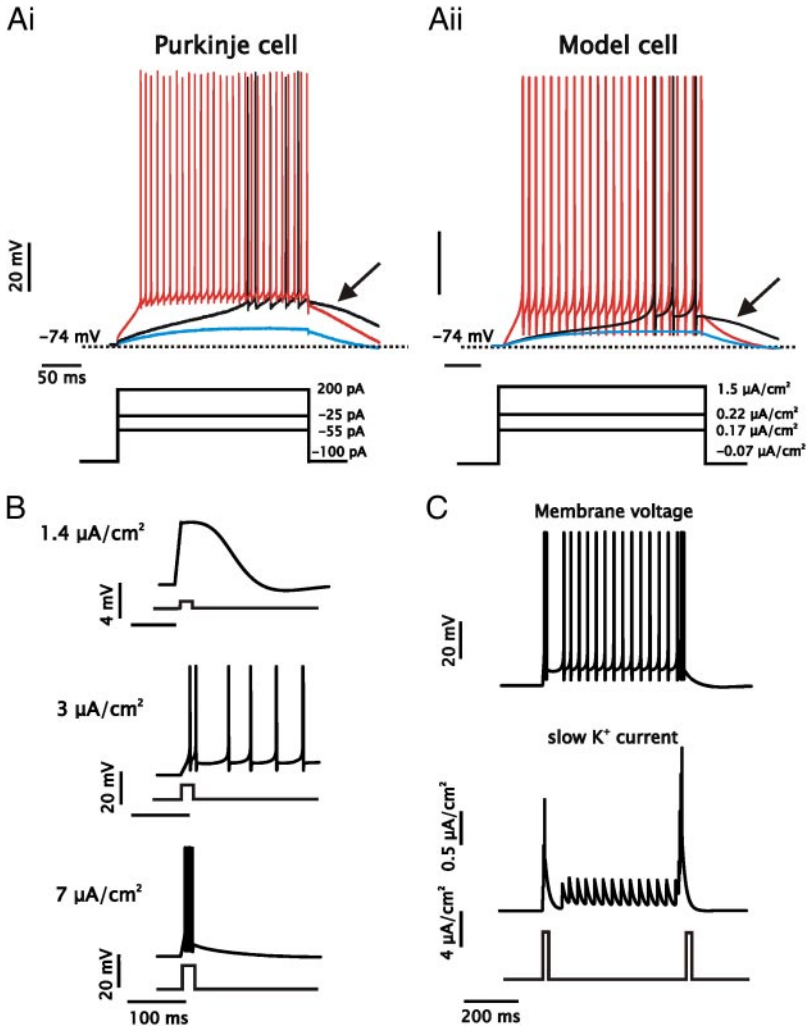

FIG. 4. Comparison of Purkinje cell and model firing behavior. *A*: Purkinje cell and model response to 3 step depolarizations of increasing magnitude [low (blue), intermediate (black), and high (red) intensities]. Purkinje cell and model were initially held at −74 mV with −100 pA and −0.07 μA/cm^2, respectively. *B*: model somatic membrane voltage response to CF-like stimuli of 3 different magnitudes (1.4, 3, 7 μA/cm^2) and 15 ms duration (initially held at −70 mV). Note that a state transition from rest to firing is achieved only for the intermediate CF-like stimulus. *C*: comparison of the time course of model somatic membrane voltage and slow K^+ current in response to 2 consecutive CF-like stimuli (4.2 μA/cm^2 and 15 ms) separated by 500 ms. Note that the presence of prior Na^+ spike firing after the transition to a firing state ensures a greater background activation of K^+ current when the second CF-like stimulus is applied. Model cell was initially held at −70 mV.

tics associated with Purkinje cell depolarization in the subthreshold range, including a long first spike latency relative to the subsequent ISI and an absence of damped oscillatory activity (Fig. 4*Aii*). The model also accurately reproduces the slow decaying plateau potential subsequent to cessation of the depolarizing current (Fig. 4*A*, *i* and *ii*). Like the Purkinje cell, the decay rate of the plateau potential is faster after greater depolarization and firing frequency (Fig. 4*A*, *i* and *ii*).

As noted previously, Purkinje cells responded to a moderate step depolarization by producing a long first spike latency that was followed by shorter ISIs (Fig. 4*Ai*). Although this behavior is similar to that of neurons expressing I_A, we established that mature rat Purkinje cells lack I_A (Supplementary Fig. 1). Rather, the I_A-like voltage trajectory in the model is explained by the fast refractory dynamics governing high-frequency firing. These dynamics can be viewed as factors equivalent to dendritic feedback, fast K^+ currents, and resurgent Na^+ current that all help maintain a depolarization after each spike. Thus by reducing the duration of the ISI, rather than lengthening the first spike latency with I_A, both Purkinje cells and the model produce a voltage trajectory similar to one with I_A.

In terms of the bistable dynamics the model is also successful in reproducing the nonmonotonic relationship between CF-like stimulation strength and state transition probability. Consequently, an intermediate stimulus of 15 ms and 3 μA/cm^2 is successful in mediating state transitions from rest to firing, whereas weaker (1.4 μA/cm^2) or stronger (7 μA/cm^2) stimuli are unsuccessful (Fig. 4*B*). Note that a weak stimulus (brief subthreshold current step) generates a substantial plateau potential lasting >100 ms (Fig. 4*B*). This is a result of the model having a saddle-node bifurcation and the corresponding steady-state Na^+ conductance in the subthreshold range required to establish the bifurcation.

Like the cell, the model is able to switch from rest to firing and from firing to rest using a strong unidirectional input (15 ms and 4.2 μA/cm^2) (Fig. 4*C*). This behavior in the model depends critically on the presence of the slow K^+ current. Thus in the presence of slow K^+ current, stimuli of intermediate strength from the rest state can transition the model to the firing state (Fig. 4*C*). Stimuli of the same strength delivered from the firing state recruits a greater amount of the slow K^+ current, which then mediates the repolarization back to the rest state (Fig. 4*C*). By comparison, without slow K^+ current a depolarizing input can transition the model only from rest to firing (not shown). Note also in Fig. 4*C* that after the initial transition from rest to spiking the onset of tonic spike firing is delayed immediately after the CF-like stimulus. A similar observation has been made in the Purkinje cell by both ourselves and others (Fig. 2*A*) (Hounsgaard and Midtgaard 1989; Williams et al. 2002). In the model this is caused by an increased activation of

the slow K^+ current after the first CF-like stimulus, which is sufficient to delay the onset of tonic spike firing (Fig. 4*C*).

To understand the dynamical and biophysical basis of bistability in the model we began by performing a single-parameter bifurcation using driving current as the bifurcation parameter. As expected, with increasing driving current the node (rest state) and saddle point coalesce at the fold (Fig. 5*A*) in a saddle-node bifurcation of fixed points. With the elimination of the rest state the system jumps onto a limit cycle attractor. Note, however, that the limit cycle exists before the coalescing of the fixed points. Within a range of driving current (Fig. 5*Aii*) the rest state is only locally stable with perturbations (such as a CF-like stimulus) capable of transitioning the system from the node to the limit cycle. If the system is already on the limit cycle, however, it remains on a periodic solution past the fold region where both a node and saddle point exist. Analysis of the frequency–current (*F–I*) relationship of the model indicates a discontinuity associated with the bistable region if the system is driven from rest to spike firing (Fig. 5*B*). Thus the lowest possible firing frequency attainable in the model if the system is driven from rest to firing is about 43 Hz. This is consistent with previous work, which has shown that the *F–I* relationship of Purkinje cells is linear and discontinuous if measured using square-wave current steps that evoke spike output ranging from threshold to high-frequency firing (Llinas and Sugimori 1980b; McKay and Turner 2005; Williams et al. 2002). If the system is driven from spike firing to rest, however, the model *F–I* relationship is continuous, albeit with a very high gain in the low-frequency range. Furthermore, our analysis indicates that bistability in the model is limited to the low-frequency and higher-gain region of the *F–I* relationship.

The bifurcation analysis and *F–I* relationship suggest that the transition from the limit cycle to the rest state is mediated by a saddle homoclinic bifurcation (as compared with a saddle-node on an invariant cycle bifurcation). In particular, the extremely high gain in the low-frequency firing range is consistent with a saddle homoclinic bifurcation (Izhikevich 2007; Rinzel and Ermentrout 1998). Also consistent with this bifurcation is the discontinuity in the *F–I* relationship when transitioning from rest to firing. Finally, a saddle homoclinic bifurcation is consistent with a bistable system that produces long first spike latencies in the absence of fast subthreshold oscillations (Izhikevich 2000, 2007; Rinzel and Ermentrout 1998). In essence a model with a saddle homoclinic bifurcation can be viewed as a system with an extremely high gain compared with one with a saddle node on an invariant cycle bifurcation. The high gain is caused by a large amount of positive feedback after a spike. If the feedback is sufficiently high (biophysically this can be generated by factors contributing to a DAP or inhibiting an AHP) any input that crosses threshold and generates a spike will cause strong positive feedback driving an additional spike and thus lead to a permanent spiking state. Under these conditions the system will be bistable and undergo a saddle homoclinic bifurcation. The saddle homoclinic bifurcation will occur when the system is taken from firing to rest with negative driving current (the bifurcation parameter). Furthermore, the gain of the *F–I* relationship in the transition from firing to rest will be extremely high.

Given that a saddle homoclinic bifurcation can be produced in a two-equation firing model (Izhikevich 2000, 2007; Rinzel and Ermentrout 1998), we proceeded to investigate whether this type of reduced model and bifurcation could account for the general behavior of Purkinje cell firing and CF-induced state transitions.

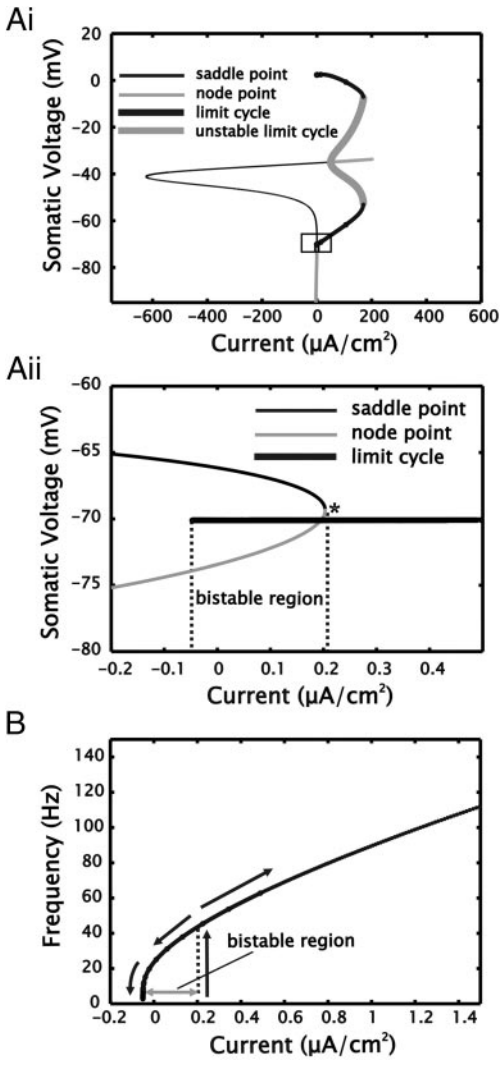

FIG. 5. Bifurcation analysis of the 5-equation model. *A*: single-parameter bifurcation diagram for somatic membrane voltage. Driving current (I_E) was used as the bifurcation parameter and was varied from −650 to 200 μA/cm^2. Stable and unstable fixed points are denoted by a thin gray and black line, respectively. Unstable limit cycle is denoted by a thick gray line. Upper and lower limits of the spike (limit cycle) amplitude are denoted by the thick black line. Note that the limit cycle and stable fixed point (thin gray line) coexist between −0.05 and 0.21 μA/cm^2 of driving current (*Aii*, boxed area in *Ai*, between dashed lines). Asterisk indicates point where a saddle-node (or fold) bifurcation of fixed points occurs. *B*: frequency–current (*F–I*) relationship for the model cell, measured between −0.05 to 1.5 μA/cm^2 of driving current. Note that the *F–I* relationship is discontinuous if the model is taken from rest to firing but continuous if taken from firing to rest. Also note that the discontinuity is associated with the end of the bistable region.

A saddle homoclinic bifurcation with a nonmonotonic separatrix can account for Purkinje cell dynamics

We started by constructing a model of two dynamical variables undergoing a saddle homoclinic bifurcation of the limit cycle. This permits phase-plane analysis such that the stable manifold of the saddle point associated with spike threshold can be visualized. Note that this is not possible with

the five-dimensional model. The phase-plane analysis also allows one to more easily discern the key biophysical features required to establish a saddle homoclinic bifurcation. In addition, it allows visualization of a separatrix, which is often associated with a bistable system. Consequently, the key requirements that control the presence and shape of the separatrix can be considered.

The two-equation model contained only a Na^+, K^+, and leak conductance. To retain the basic biophysics of spike firing using only two equations we let Na^+ conductance activation equilibrate instantaneously with membrane voltage and modeled Na^+ inactivation and K^+ activation using the same variable (Rinzel 1985). Consequently, the two dynamical variables are membrane voltage and refractoriness (representing both K^+ activation and Na^+ inactivation). Previous work has established that a saddle homoclinic bifurcation and the resulting bistability can be achieved using a refractory time constant that is small relative to the membrane time constant (Izhikevich 2000, 2007; Rinzel and Ermentrout 1998). We manipulated leak conductance density (to adjust the membrane time constant) and the refractory time constant to establish a saddle homoclinic bifurcation. We set the default value for the refractory time constant at 0.6 ms. Although this value suggests a very fast K^+ current, recent voltage-clamp data from Purkinje cell nucleated patches has measured and confirmed the presence of a fast and prominent K^+ conductance (Martina et al. 2007).

In Fig. 6*A* we show the phase-plane projection of the model for three different time constants of the refractory variable. When the model has a large time constant for the refractory variable (1.2 ms) the transition from the limit cycle to the stable fixed point is mediated by a saddle node on an invariant cycle bifurcation. As a consequence the system has no bistable dynamics and the stable manifold (dashed line) of the saddle point connects to the unstable point on its right (Fig. 6*Ai*). As the refractory time constant is reduced to an intermediate value (0.6 ms), however, the system undergoes a saddle homoclinic bifurcation of the limit cycle. Under this condition the stable manifold becomes a separatrix, which separates two regions in phase space that correspond to the two possible steady-state solutions (rest and firing) of the model (Fig. 6*Aii*). A separatrix can be viewed as a line in phase space corresponding to a demarcation of a hard threshold. Thus any perturbation that crosses the separatrix in a bistable system will result in a transition to the firing or rest state depending on the current state of the model. In a nonbistable system undergoing a saddle-node bifurcation the stable manifold simply demarcates the firing threshold of the model. Note that with a saddle homoclinic bifurcation a single spike is capable of generating a large depolarizing afterpotential (DAP) as a consequence of the fast refractory dynamics (Fig. 6*B*). Also important is the shape of the separatrix. Because the separatrix is nonmonotonic, such that it surrounds the limit cycle, a unipolar input can be used to switch between the stable point and the limit cycle (Fig. 6*C*). For this reason intermediate inputs can switch the model from the rest state to the firing state, whereas excessively strong inputs fail because they cross the separatrix twice, bypassing the firing state and returning the system to the rest state. This provides a dynamical systems explanation of the restricted range of CF-like stimuli that are able to induce state transitions in the bistable region. If the refractory time constant

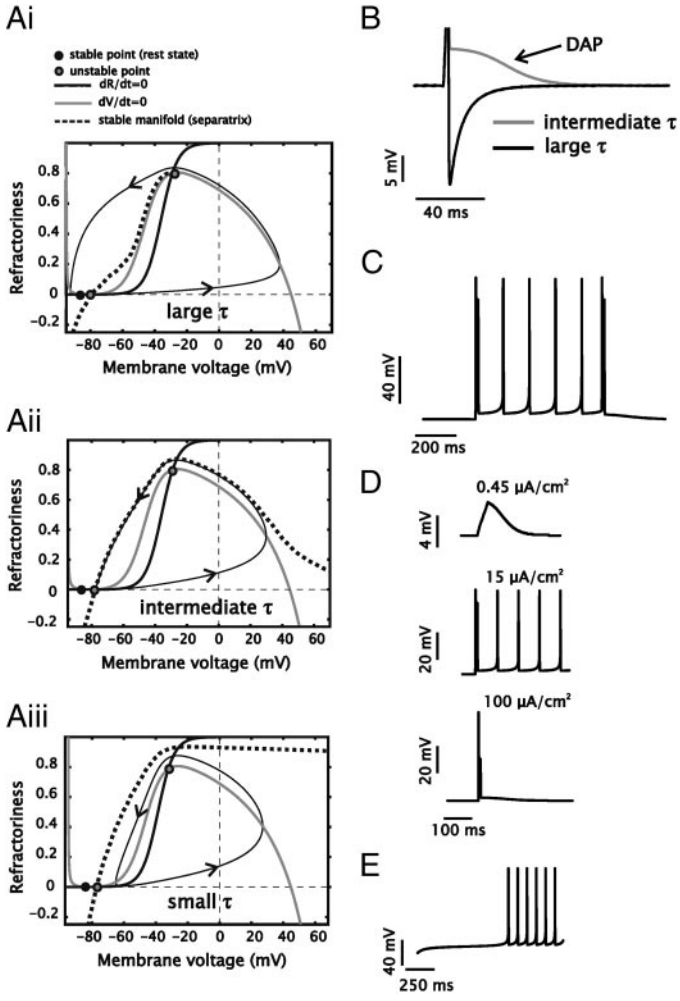

FIG. 6. Phase-plane analysis of the 2-equation model undergoing a saddle homoclinic bifurcation. *A*: phase-plane projection for the model with a large (1.2 ms, *Ai*), intermediate (0.6 ms, *Aii*), or small (0.2 ms, *Aiii*) refractory time constant. Black and gray lines denote the refractory and voltage nullclines, respectively. Limit cycle is denoted by the thin black line, with arrows indicating direction of flow. Dashed lines denote the stable manifold (a separatrix in *Aii* and *Aiii*) of the saddle point (*middle point*). *B*: voltage trajectory for model after a brief (2-ms) current step (11.25 $\mu A/cm^2$) using a slow (black line, 1.2 ms) or intermediate (gray line, 0.6 ms) refractory time constant. Model was initially held at −73 mV with 0.257 $\mu A/cm^2$. *C*: model cell response to 2 consecutive CF-like stimuli (140 $\mu A/cm^2$, 15 ms) separated by 500 ms using an intermediate refractory time constant. Model cell was initially held at −71 mV. *D*: model cell response to CF-like stimuli of 3 different magnitudes (1, 15, and 150 $\mu A/cm^2$, 15 ms). Model was initially held at −73 mV. Note that only the intermediate-size CF-like stimulus is successful in inducing state transitions. *E*: model cell response to a step depolarization from 0 to 0.55 $\mu A/cm^2$. Note that the first spike latency is longer than the subsequent ISI.

is further reduced (0.2 ms) the model retains the saddle homoclinic bifurcation and bistability but the separatrix becomes monotonic (Fig. 6*Aiii*). Thus switching from the rest state to the limit cycle can be done with a positive current input, whereas switching from the limit cycle to the rest state requires a negative current input. Note that when the model has a saddle homoclinic bifurcation it generates a long first spike latency relative to the subsequent ISI (Fig. 6*E*). This is a consequence of the fast refractory dynamics, which actively shorten the ISI relative to the first spike latency, and is consistent with our previous interpretation of the five-equation model.

Our two-equation model indicates that, from a biophysical perspective, any factors that provide a net depolarizing influence after spike generation can potentially establish a saddle homoclinic bifurcation and bistability. In effect, the bistability emerges because spike generation is followed by a depolarization or weak hyperpolarization, which locks the system into a spike firing solution. As a result, over a range of current input, spike firing becomes self-generating once threshold is crossed. In the two-equation model the primary cause of bistability is the fast deactivation of the K^+ conductance, which prevents the system from fully resetting once threshold is crossed. Also important is the membrane time constant. A comparatively long membrane time constant acts in a manner similar to that of a fast deactivating K^+ conductance because it prevents the membrane from fully resetting after spike generation by retaining membrane charge for a long duration. An intermediate refractory time constant, however, is required for state transitions to be mediated by a unipolar input. This is similar to the addition of a slow K^+ current in the five-equation model, which permits a CF-like stimulus to mediate state transitions.

Biophysical basis for bistability in the five-equation model

In the five-equation model dynamics similar to those present in the two-equation model should establish bistability, although additional factors will be important. The two-equation model, however, predicts that the presence of conductances that slow membrane repolarization and increase the membrane time constant will establish a saddle homoclinic bifurcation and bistability. Thus we predict that removing the dendritic compartment and reducing Na^+ conductance will eliminate bistability by removing a spike-dependent depolarizing factor (dendritic feedback) and decreasing the membrane time constant (Na^+ conductance removal). Alternatively, increasing the K^+ conductance and leak conductance will eliminate bistability by producing a strong and long-duration hyperpolarization after a spike and decreasing the membrane time constant (arising from the increased leak conductance).

To test these predictions in the five-equation model we proceeded to manipulate the components predicted to establish a saddle homoclinic bifurcation and control the bistable range. We performed a bifurcation analysis under each manipulation to evaluate overall system dynamics. We considered four factors: the dendritic compartment, refractory dynamics, leak conductance, and the Na^+ window current. For each parameter we considered the scenario that would be predicted to reduce the bistable range. Thus we removed the dendritic compartment, slowed the refractory variable, increased somatic leak conductance, and reduced the Na^+ window current (through a -6 mV shift in the steady-state inactivation parameter). As shown in Fig. 7, *A–E* each of the manipulations reduces or eliminates the bistable range of the model (indicated by a reduced overlap between the limit cycle and node across different current values). Under the control condition (Figs. 5 and 7*A*) the bistable range occurs over 0.26 μA/cm^2 of driving current. Under each of the four manipulations the bistable range is either eliminated or reduced to $<$0.03 μA/cm^2 range of driving current (Fig. 7, *B–E*).

To further illustrate the effects of these four manipulations on bistability we considered the DAP after a single spike. As stated previously, the factors analyzed here contribute to bistability by providing a depolarization after each spike, which locks the system into a spike firing solution. Below the bistable range (when the model is slightly hyperpolarized), however, it is expected that the model will generate a DAP before returning to the rest state and that any of the four manipulations described earlier will reduce the size of the DAP. As shown in Fig. 7*Fi*, the control model (black line) produces a large DAP after a brief current step. Conversely, any of the manipulations that reduce the bistable range also reduce or eliminate the DAP (Fig. 7*Fi*). Furthermore, when the model is held at a more depolarized membrane potential (-70 mV, within the bistable region) the ability to switch from rest to firing is eliminated with any of the four manipulations (Fig. 7*Fii*).

The five-equation model can account for previous experimental results

As a test of the validity of our model we sought to examine whether it could reproduce previous experimental results related to bistability that remain unexplained. In particular, we were interested in the effects of changing the density of Na^+ current on plateau potentials and the density of I_H on the bistability range.

Previous work has established that a small reduction of Na^+ conductance with TTX in Purkinje cells can reduce the duration of spiking plateau potentials with no effect on spike parameters (Williams et al. 2002). We proceeded to reduce the Na^+ conductance density ($g_{Na_{max}}$) and test the ability of the model to generate plateau potentials in response to a brief current step. We note that in the model the plateau potential is generated by the same factors that sustain the DAP. For these simulations the model was held at -73 mV with 0.023 μA/cm^2. As shown in Fig. 7, a small reduction in $g_{Na_{max}}$ that reduces the DAP shortens the duration of the spiking plateau potential (Fig. 7*G*, *i* and *ii*). Because the plateau potential is caused by a balance of inward and outward currents, a small change in $g_{Na_{max}}$ has a dramatic effect on its duration, eventually eliminating the ability to generate a plateau potential and bistability. In contrast, during the spike upstroke membrane permeability is dominated by Na^+ conductance. As a result, a small change in $g_{Na_{max}}$ has no effect on spike parameters (Fig. 7*Gii*). Thus our model can accurately reproduce these experimental observations within the biophysical context described previously to establish a saddle homoclinic bifurcation.

We next examined the effects of I_H on the bistable range of the model. The effect of I_H on bistability remains somewhat controversial. Experimental results indicate that removal of I_H with pharmacological blockers or modulators does not inhibit bistability (Williams et al. 2002). In fact, the overall effect of I_H block is to increase the observation of bistability in Purkinje cells (Williams et al. 2002). Modeling data from a more recent study, however, place I_H as the critical conductance underlying bistability in Purkinje cells (Loewenstein et al. 2005). Given that only modeling data suggest a critical role for I_H in sustaining bistability (Loewenstein et al. 2005), we carried out experiments to examine the effects of removing I_H with 20 μM 4-(*N*-ethyl-*N*-phenylamino)-1,2-dimethyl-6-(methylamino) pyridinium chloride (ZD7288) on bistability. To test for bistability cells were held at -68 mV and given two 15 ms duration 2 nA current steps of positive and then negative polarity spaced 500 ms apart (Fig. 8*Ai*). In all cells tested ($n = 8$) blockade of

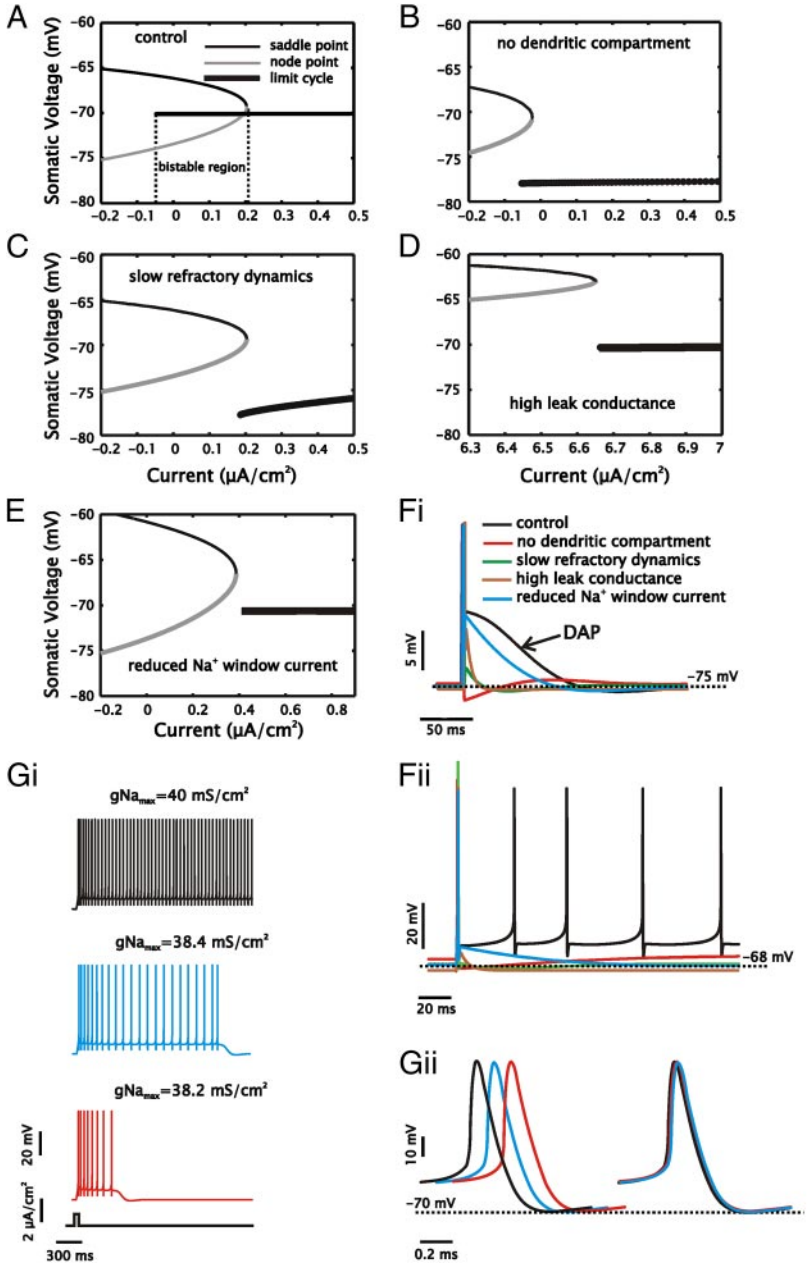

FIG. 7. Biophysical parameters establishing a saddle homoclinic bifurcation and bistability in the 5-equation model. *A–E*: bifurcation diagram as a function of driving current for the model under 5 different conditions: control (*A*), no dendritic compartment (*B*), slow refractory dynamics (*C*), high leak conductance (*D*), and reduced Na^+ window current (*E*). Stable and unstable fixed points are denoted by a thin gray and black line, respectively. Lower limit of the spike (limit cycle) amplitude is denoted by the thick black line. To establish slow refractory dynamics the time constant function for the somatic refractory variable was multiplied by 2. For high leak conductance the base maximal leak was multiplied by 10. To establish a smaller window current for Na^+ conductance the steady-state inactivation parameter was shifted by −6 mV. *F*: superimposed membrane voltage responses of the model under the 4 different conditions indicated in *A–E* when driven with a brief current pulse (2 ms, 30 $\mu A/cm^2$) and initially held near −75 mV. Note that under all 4 conditions the size of the depolarizing afterpotential (DAP) is reduced from control. When held at a more depolarized potential (near −68 mV, *Fii*) and given the same stimulus as in *Fi* all 4 manipulations prevent a transition from rest to firing that occurs under control conditions (black line). *G*: duration of spiking plateau potentials and spike shape under different maximal Na^+ conductances ($g_{Na_{max}}$). Under the control condition ($g_{Na_{max}}$ = 40 mS/cm², black line) a transient current step (1 $\mu A/cm^2$, 20 ms) is sufficient to transition the system from rest to firing when the model is held at −73 mV with 0.023 $\mu A/cm^2$. With small reductions in $g_{Na_{max}}$ to 38.4 mS/cm² (blue line) or 38.2 mS/cm² (red line) the duration of the plateau potential is reduced and the system can no longer transition permanently to the firing state. Note that despite differences in $g_{Na_{max}}$ values the spike shape is conserved, as shown in *Gii* with superimposed traces.

I_H did not prevent state transitions between rest and firing (Fig. 8*Ai*). Thus bistability was not blocked by the removal of I_H, confirming previous results by Williams et al. (2002). An effective block of I_H was confirmed by delivering a negative 2 nA current pulse (15 ms), which under control conditions produced a voltage overshoot and dampening (indicating deactivation of I_H) that was abolished in the presence of 20 μM ZD7288 (Fig. 8*Aii*).

To examine the role of I_H in the model we changed the I_H conductance density and measured the bistable range using a bifurcation analysis. In Fig. 8*B* we show the effects of four different I_H conductance densities [0.03 (control), 0, 0.06, and 0.3 mS/cm²] on the bistable range of the model. With the complete removal of I_H the bistable range increases by a small amount relative to the control case (Fig. 8*Bii*), whereas an increase in I_H decreases the bistable range (Fig. 8*B*, *iii* and *iv*). We followed by plotting the bistable range of the model as a function of I_H density (Fig. 8*C*). As indicated, the effect of adding I_H is to decrease the bistable range of the model over a large range of conductance densities (Fig. 8*C*).

Although I_H might be expected to increase the bistable range of the neuron by contributing to the DAP (by rebounding membrane voltage during the spike AHP), its major contribution to membrane dynamics comes about through a decrease in input resistance and the membrane time constant. This occurs because the time constant of I_H activation and deactivation is too large for any dynamic contribution during a single spike cycle. Consequently, only the steady-state activation of I_H contributes to the bistable dynamics by decreasing the membrane time constant and decreasing the amplitude and duration of the DAP (Fig. 8*D*). In fact, data in support of this have been reported, in that blockade of I_H with ZD7288 has been shown to increase input resistance and the membrane time constant (Williams et al. 2002). Thus within the context of the saddle homo-

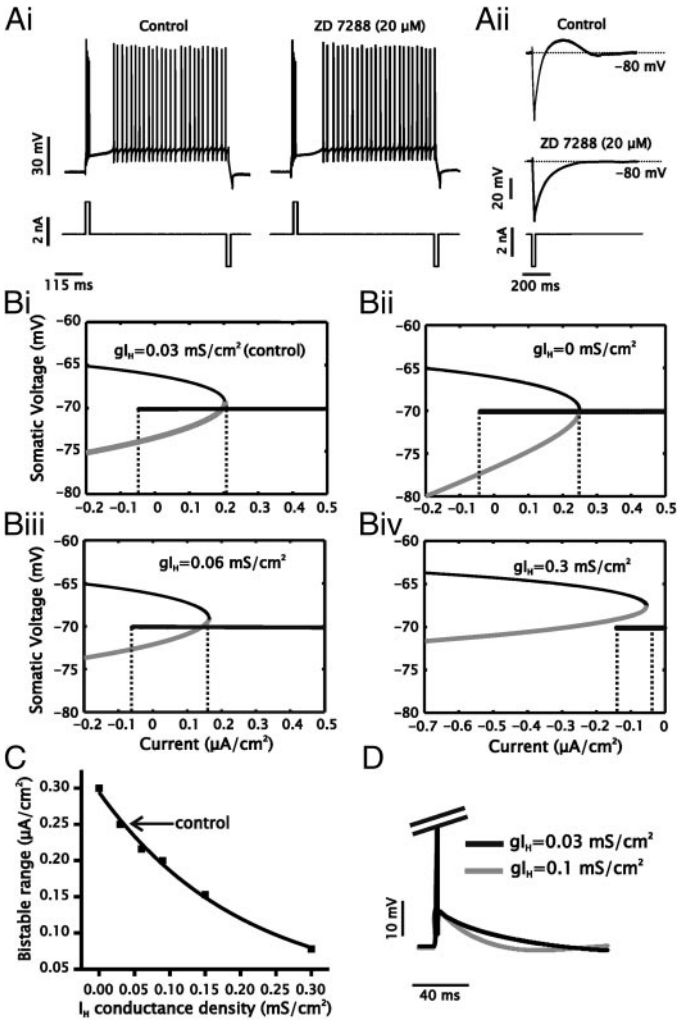

FIG. 8. Effect of a hyperpolarizing activated cation current (I_H) on bistability in the Purkinje cell and 5-equation model. *A*: representative membrane voltage response of a Purkinje cell given two 15 ms duration 2 nA current steps of positive and then negative polarity spaced 500 ms apart with or without 20 μM bath-applied 4-(*N*-ethyl-*N*-phenylamino)-1,2-dimethyl-6-(methylamino) pyridinium chloride (ZD7288, *Ai*). Removal of I_H is confirmed with a negative 2 nA current step of 15-ms duration (*Aii*) and loss of a sag in the membrane hyperpolarization. *B*: bifurcation diagram as a function of driving current for the model under 4 different I_H conductance densities (g_{I_H}; in mS/cm^2): 0.03 (*Bi*, *control*), 0 (*Bii*), 0.06 (*Biii*), and 0.3 (*Biv*). Stable and unstable fixed points are denoted by a thin gray and black line, respectively. Lower limit of the spike (limit cycle) amplitude is denoted by the thick black line. *C*: plot of the bistable range of the model as a function of I_H conductance densities. Bistable range was calculated using a bifurcation analysis for g_{I_H} values ranging from 0 to 0.3 mS/cm^2. *D*: membrane voltage response of model under 2 different g_{I_H} values when driven with a brief 2 ms current pulse (30 μA/cm^2) and initially held at -75 mV (requiring -0.1 μA/cm^2 with 0.03 mS/cm^2 g_{I_H} and -1 μA/cm^2 with 0.1 mS/cm^2 g_{I_H}). Note that the reduction of g_{I_H} increases the duration of the DAP.

clinic bifurcation the addition of I_H is equivalent to an increase in leak conductance and a shorter membrane time constant.

Testing model predictions in Purkinje cells

To further evaluate the validity of our model we proceeded to test some of the predictions made by the model. We considered the following qualitative behaviors: the presence of a DAP during antidromic stimulation, high gain in the low-frequency firing region of the *F–I* relationship, and a bistable range limited to the low-frequency firing range.

A critical feature to establishing a saddle homoclinic bifurcation in our model is the presence of a long DAP. To test whether Purkinje cells produce a DAP similar to that observed in the model we used antidromic stimulation to elicit a single spike during whole cell Purkinje cell recordings. Cells were held between -80 and -65 mV and stimulated antidromically with a bipolar electrode in the white matter region of the folia in the presence of synaptic blockers (see METHODS). All Purkinje cells tested produced a substantial DAP lasting between 50 and 100 ms and ranging in amplitude from 3 to 7 mV (Fig. 9*Aii*; $n = 4$). The voltage trajectory of the Purkinje cell DAP thus compared favorably with that of the model when driven with a brief 2 ms current step.

A second prediction made by the model is that Purkinje cells should be able to fire at low firing frequencies and that the gain (slope) of the *F–I* relationship should be significantly higher at low frequencies. In the model this occurs because the system undergoes a saddle homoclinic bifurcation, which produces a high-gain region in the bistable range of the neuron. To test this we applied a ramp protocol that carried the cell from rest to firing and back to rest. The total duration of the ramp was 4 s with a slope of 100 pA/s (cells were initially held at approximately -75 mV). As shown in a previous study (Williams et al. 2002), Purkinje cells respond to a ramp protocol with strong hysteresis (Fig. 9*Bi*). Thus all cells tested were able to fire spikes at lower current inputs on the downstroke than on the upstroke of the ramp. To measure the gain of the cell during the ramp we constructed an *F–I* relationship from the instantaneous firing frequency during the protocol (Fig. 9*B*, *ii* and *iii*). In all cells tested, the lowest attainable frequency was lower on the downstroke than on the upstroke of the ramp protocol (Fig. 9*B*, *ii* and *iii*; $n = 7$). Indeed, in many cases Purkinje cells could be made to fire at a frequency <20 Hz on the downstroke of the ramp protocol when the same cells would typically begin to fire between 60 and 70 Hz on the upstroke. Note that the lower frequency value obtained during the downstroke is also significantly lower than the onset frequency reported by previous studies, which normally measure the *F–I* relationship using current steps that take the cell from rest to firing (Llinas and Sugimori 1980b; McKay and Turner 2005; Womack and Khodakhah 2002). Furthermore, a measurement of the gain of the *F–I* relationship using a linear fit indicated that gain was significantly higher at lower firing frequencies (<50 Hz) (Fig. 9, *C* and *D*; $P < 0.01$, $n = 7$), a result consistent with our model. A recent study has also shown that evoked or simulated parallel fiber excitatory postsynaptic potentials (EPSPs) have a higher gain (produce a larger change in firing frequency) when applied at low firing frequencies (<60 Hz) relative to those applied at high firing frequencies (>60 Hz) in Purkinje cells (McKay et al. 2007).

Another key property in our model is that bistability is limited to the low frequency firing region (<43 Hz). With increased driving current and firing frequency, the stable rest state (node) disappears by a saddle-node bifurcation, leaving the limit cycle as the globally stable solution. Consequently, Purkinje cells should be able to transition between the firing and rest state only at low firing frequencies. We tested this by holding Purkinje cells at two different ranges of firing frequency and using an inhibitory current step that hyperpolarized

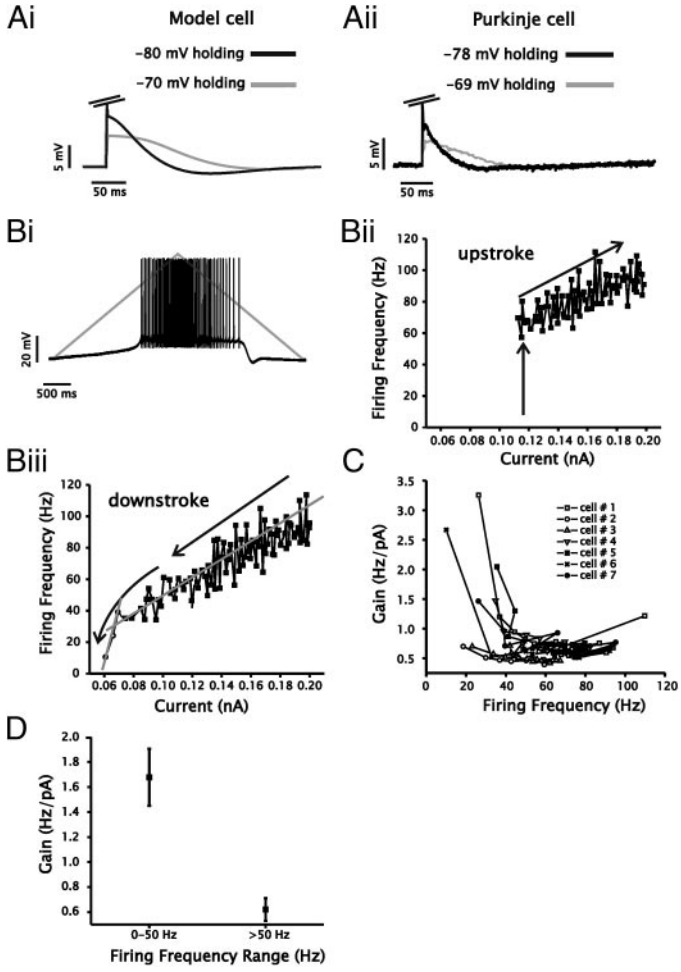

FIG. 9. Presence of a DAP and a nonlinear *F–I* relationship in Purkinje cells confirms model predictions. *A*: antidromic stimulation of Purkinje cells when holding the cell at 2 different membrane potentials: −78 mV (black line) and −68 mV (gray line). For comparison the voltage trajectory for the 5-equation model after a brief current step (30 μA/cm^2, 2 ms) when initially held at −80 mV (black line) and −70 mV (gray line) is shown in *Ai*. *B*: hysteresis and *F–I* relationship at low and high firing frequencies in Purkinje cells. Purkinje cells were held at −75 mV and given a ramp protocol lasting 4 s (2 s on each side) with a slope of 100 pA/s (*Bi*). Note that Purkinje cells respond to the ramp protocol with strong hysteresis (*Bi*) in exhibiting the ability to fire for lower current inputs on the downstroke of the current-ramp protocol. Plots of the *F–I* relationships are shown calculated during the upstroke (*Bii*) and downstroke (*Biii*) of the ramp. Frequency was calculated as the inverse of the instantaneous ISI. *C*: plot of instantaneous gain as a function of firing frequency for 7 different Purkinje cells determined using the ramp protocol described earlier. *D*: average gain of the *F–I* relationship was significantly higher in the low frequency region (<50 Hz) compared with the high frequency region (>50 Hz; $P < 0.01$, $n = 7$). Frequency was measured as the average firing frequency within the given range.

the cell to −90 mV ($n = 6$). We used inhibitory rather than excitatory current steps to induce the transition from firing to rest because it was easier to control the final membrane voltage (we defined a low firing frequency as <50 Hz). When Purkinje cells fired at low frequencies a hyperpolarizing step of 85 ms duration was sufficient to transition the cell from firing to rest (Fig. 10). Conversely, when Purkinje cells were held at high firing frequencies a similar step (we increased the size of the inhibitory current step to take the cell to the same final membrane voltage) was insufficient to transition the system from firing to rest. We also carried out these experiments with positive current steps (5 nA) and found that bistability was limited to the low firing frequency range (data not shown). Thus these tests validate the basic dynamics of our model and provide novel information on Purkinje cell firing behavior.

DISCUSSION

The current study identifies two different bifurcations that can account for several established properties of cerebellar Purkinje cell firing. Although in this study we do not indicate all the precise factors likely to contribute to Purkinje cell bistability, we delineate the basic biophysical and dynamical mechanisms by which it is achieved. In doing so we provide a general framework from which future studies can determine all the possible contributing factors. Within this framework we account for previous observations and reproduce them accurately using our model. Furthermore, we use our model, dynamic systems analysis, and experimental data to demonstrate and explain important and even previously unrecognized aspects of Purkinje cell firing behavior. These include the following properties: a narrow range of a CF-like stimulus is capable of transitioning Purkinje cells to the firing state, spike firing at frequencies <40 Hz, a nonlinear *F–I* relationship with a high gain in the low frequency region, and that the bistable region is limited to the low-frequency firing range. These findings are significant because they indicate that numerous properties of Purkinje cell firing are fundamentally linked to the type of bifurcation underlying threshold transitions in the cell. As a result, we find that bistability is one of many properties associated with the presence of a saddle homoclinic bifurcation in Purkinje cells.

Biophysical basis of bistability in Purkinje cells

Because bistable dynamics in Purkinje cells emerge through a saddle homoclinic bifurcation, the basic factors controlling bistability are the membrane time constant and the spike refractory dynamics that generate a DAP. Within the bistable range the DAP provides sufficient depolarization after the spike to generate an additional spike and permanently stabilize tonic firing. In essence, the DAP can be viewed as equivalent to the excitatory feedback used in some models of network activity that produce bistability and persistent activity (Li et al. 2006; Seung et al. 2000). Consequently, any factors that decrease the membrane time constant and/or slow the refractory dynamics will reduce or eliminate the DAP and bistability. In Purkinje cells a major contributing factor to bistability is the long membrane time constant, which is likely to result from a large specific membrane resistance (Rapp et al. 1994; Roth and Hausser 2001). The long membrane time constant acts to slow the final repolarization after a spike and thus contributes to the DAP. Similarly, a fast refractory variable contributes to a DAP by turning off sufficiently fast as to permit a depolarization to dominate the postspike period. Numerous factors can contribute to a fast refractory variable. These include fast deactivating K^+ currents or resurgent Na^+ current. A resurgent Na^+ current could support a DAP because this type of conductance activates during the repolarizing phase of a spike. Consequently, the presence of a resurgent Na^+ current can be viewed as similar to a fast deactivating K^+ current because both types of currents can shorten the effective refractory period and support

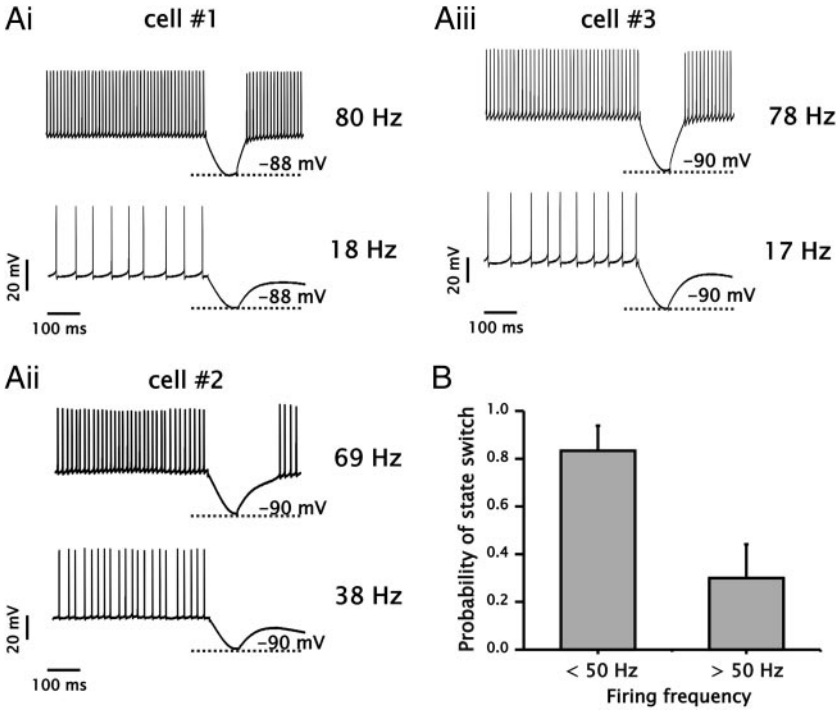

FIG. 10. Bistability is limited to the low frequency firing range in Purkinje cells. *A*: representative examples of the voltage trajectory for 3 different Purkinje cells responding to 85 ms negative current steps ranging from −300 to −700 pA. Cells were held at 2 different ranges of steady-state firing frequencies corresponding to low (<50 Hz) and high (>50 Hz) with holding current ranging from 80 to 200 pA. Note that successful transitions from the firing to the rest state are more likely to occur when a cell is in the low frequency firing regime. *B*: plot of the probability of evoking a state transition from firing to rest determined using 10 stimulations at the indicated baseline firing frequency using the protocol described in *A*. Average probability for a successful state transition was higher at a lower baseline firing frequency compared with baseline firing frequencies >50 Hz ($P < 0.01$, $n = 6$).

a DAP. Although we did not include a resurgent Na^+ current in any of our models, its presence would accentuate the dynamics described in this study and would thus contribute to establishing a saddle homoclinic bifurcation. In support of this, previous studies have shown that Purkinje cells express both of these types of currents (Martina et al. 2003; McKay and Turner 2004; Raman and Bean 2001).

As indicated by our model, Purkinje cell dendrites should also contribute to the DAP. Because dendritic voltage is more positive than the soma immediately after a Na^+ spike (McKay and Turner 2004; Stuart and Hausser 1994), current can flow into the soma and contribute to a late depolarization. As a result, when combined with a long membrane time constant and fast refractory dynamics, a dendritic compartment contributes to establishing bistability.

A past study on the development of Purkinje cell morphology and in vitro electrophysiological properties is also consistent with our interpretation and model (McKay and Turner 2005). In particular, this study showed that the ability to generate a discontinuous *F–I* relationship, a first spike latency longer than the subsequent ISI, and bistability develops in parallel with the generation of a narrower somatic Na^+ spike and larger dendritic arbor. This suggests that the development of a dendritic arbor and fast refractory dynamics contribute to establishing properties associated with a saddle homoclinic bifurcation.

Although Purkinje cell dendrites have been shown to generate Ca^{2+} spikes and Ca^{2+}-dependent plateau potentials (Llinas and Sugimori 1980a), dual recordings from soma and dendrite indicate a lack of Ca^{2+} spike activity during tonic somatic Na^+ spike firing (0–200 Hz) (McKay and Turner 2004; Stuart and Hausser 1994; Williams et al. 2002). This is also consistent with dendritic recordings from Llinas and Sugimori (1980b), which show Ca^{2+} spikes only during burst firing or with strong local depolarization of the dendrite with current steps. Furthermore, previous work has indicated that blocking voltage-gated Ca^{2+} conductances does not decrease bistability (Williams et al. 2002). Consequently, Ca^{2+} spikes and Ca^{2+}-mediated plateau potentials may represent a local dendritic phenomenon required for synaptic integration, but have less influence on the intrinsic somatic firing dynamics within the *tonic* firing range.

A previous reduced model of Purkinje cells used an I_H conductance measured in entorhinal cortical stellate cells to reproduce membrane voltage bistability associated with CF-like stimulation (Loewenstein et al. 2005). Although this model captures some of the elements of Purkinje cell dynamics, such as switching with a unipolar current input, it fails to account for experiments that indicate that block of I_H does not eliminate bistability and can actually augment the bistable range (Williams et al. 2002). Because the Loewenstein model has no spiking dynamics, bistability results from a relatively slow variable (I_H activation and deactivation) and I_{Na}. It is assumed in this model that the introduction of fast spiking dynamics will not change this and that spikes will ride on top of the I_{Na}-I_H-mediated plateau potential. Consequently, bistability in the Loewenstein model is between two different rest states (hyperpolarized and depolarized).

Both models presented in the current study differ critically in this respect. First, bistability is between a rest state and a firing state. Second, bistability depends on the fast variables in the model that are within the timescale of a single spike. The following information, however, supports our current models. Most important is the fact that I_H block does not eliminate bistability in Purkinje cells, but rather can increase the observation of bistability in these cells. Purkinje cell bistability has been shown to be eliminated with TTX (Williams et al. 2002), thus supporting the conclusion that bistability is between a rest state and a firing state. We should also note that we observed no bistability in membrane voltage (between two rest states) once spiking had been abolished with 1 μM TTX. Finally, Purkinje cells have been shown to have fast refractory dynam-

ics consistent with our biophysical and dynamical interpretation. Thus we feel that our current models represent a more biophysically and dynamically accurate explanation of Purkinje cell firing behavior.

Spontaneous activity in vitro

Previous studies in vitro have delineated two types of spontaneous activity in Purkinje cells. The first type is tonic firing, which can vary in frequency from 70 to 200 Hz (Williams et al. 2002). The second type is a trimodal burst firing pattern, which consists of a three-stage cycle: tonic firing, burst firing, and quiescence (McKay and Turner 2004; Womack and Khodakhah 2002). In our present work we found that more than half the cells expressed a trimodal firing pattern, whereas the rest of the cells fired tonically with no indication of trimodal activity. Details on the prevalence and development of intrinsic trimodal activity in Purkinje cells were recently described (McKay and Turner 2005). In the current study the trimodal pattern was sidestepped for the duration of experiments by applying a slightly negative bias current to reduce the rate of Na^+ spike firing. Given the exceedingly complex nature of the dynamics associated with trimodal burst firing we did not include them in our model. Moreover, we recently showed that reintroducing a physiological rate of CF-like stimuli and complex spike depolarizations in vitro rapidly blocks trimodal activity and slows Na^+ spike frequency to the range necessary to observe bistable behavior and the associated change in gain now explained mechanistically here (McKay et al. 2007).

Low firing frequency

Previous in vitro work on Purkinje cells has established that the *F–I* relationship is linear and discontinuous with a minimal firing frequency ranging from 40 to 70 Hz using standard current step protocols (Llinas and Sugimori 1980b; McKay and Turner 2005; Williams et al. 2002). Our model and data indicate that the *F–I* relationship of Purkinje cells is nonlinear and has a firing frequency range substantially $<$40 Hz. The low frequency firing range, however, occurs largely within the bistable range. As a consequence the only way to attain low firing frequencies is to impose a hyperpolarizing shift (i.e., with negative current) once the cell has *already* attained a high frequency firing state. Alternatively, CF-like stimuli at rest can transition the system to the low frequency firing range because bistability is limited to that range of frequencies.

Comparison to in vivo Purkinje cell firing behavior

Recent work in rat cerebellum has shown that bistability can be observed in vivo (Loewenstein et al. 2005), although there is controversy as to whether CF-induced toggling between states reflects natural or experimental conditions (Schonewille et al. 2006). Our analysis of Purkinje cell dynamics indicates that only intermediate-strength CF-like stimuli can mediate state transitions. In this regard, direct recordings in vitro indicate a substantial variation in the net current evoked during a CF-evoked complex spike depolarization between different Purkinje cells, suggesting that CF-induced toggling may be more prevalent in cells receiving CF postsynaptic currents in the appropriate range (McKay et al. 2005). Additionally, the bistable area of Purkinje cells is limited to the low frequency firing region. Thus the restrictions placed by the requirement of a complex spike of the correct magnitude and a limited bistable range may render state transitions induced through CF activation less likely to be encountered in awake animals, but still potentially active when the appropriate conditions are met.

Our analysis further indicates that switching between the two states is only one of many features associated with intrinsic Purkinje cell dynamics. Although bistability is the most obvious of characteristics with a potential functional significance associated with a saddle homoclinic bifurcation, many of the other properties associated with this bifurcation may also be important. First spike latencies longer than the subsequent ISI, plateau potentials (both spiking and nonspiking), and a discontinuous *F–I* relationship in the slow transition from rest to firing are also a consequence of a saddle homoclinic bifurcation. Some, if not all, these features may be important for in vivo Purkinje cell function even under conditions in which CF activation remains unable to toggle between a rest and firing state. For example, the high gain at lower firing frequencies would still be influential in vivo, a condition that could be established when tonic CF activation reduces Purkinje cell firing rate (Cerminara and Rawson 2004; Colin et al. 1980; McKay et al. 2007; Montarolo et al. 1982). This has previously been suggested to reflect the activation of Ca^{2+}-dependent K^+ channels by the complex spike depolarization (Cerminara and Rawson 2004; Hounsgaard and Midtgaard 1989; McKay et al. 2007), indicating that the history of CF input will be important in actively regulating the gain of the cell. Indeed, work in vivo has shown that Purkinje cell responsiveness to excitatory and inhibitory stimuli is increased after CF activation (Ebner and Bloedel 1981, 1984). The dynamical and biophysical basis for bistability in Purkinje cells delineated here may then be important to understanding multiple aspects of Purkinje cell output.

ACKNOWLEDGMENTS

We gratefully acknowledge the technical assistance of M. Kruskic, M. L. Molineux, and B. E. McKay and comments on the manuscript by W. H. Mehaffey.

GRANTS

This work was supported by a Canadian Institutes of Health Research (CIHR) Doctoral Studentship to F. R. Fernandez and CIHR operating grant and Alberta Heritage Foundation for Medical Research Scientist Award to R. W. Turner.

REFERENCES

Cerminara NL, Rawson JA. Evidence that climbing fibers control an intrinsic spike generator in cerebellar Purkinje cells. *J Neurosci* 24: 4510–4517, 2004.

Colin F, Manil J, Desclin JC. The olivocerebellar system. I. Delayed and slow inhibitory effects: an overlooked salient feature of cerebellar climbing fibers. *Brain Res* 187: 3–27, 1980.

Crunelli V, Toth TI, Cope DW, Blethyn K, Hughes SW. The "window" T-type calcium current in brain dynamics of different behavioural states. *J Physiol* 562: 121–129, 2005.

De Schutter E, Bower JM. An active membrane model of the cerebellar Purkinje cell II. Simulation of synaptic responses. *J Neurophysiol* 71: 401–419, 1994a.

De Schutter E, Bower JM. Simulated responses of cerebellar Purkinje cells are independent of the dendritic location of granule cell synaptic inputs. *Proc Natl Acad Sci USA* 91: 4736–4740, 1994b.

Doiron B, Longtin A, Turner RW, Maler L. Model of gamma frequency burst discharge generated by conditional backpropagation. *J Neurophysiol* 86: 1523–1545, 2001.

Ebner TJ, Bloedel JR. Role of climbing fiber afferent input in determining responsiveness of Purkinje cells to mossy fiber inputs. *J Neurophysiol* 45: 962–971, 1981.

Ebner TJ, Bloedel JR. Climbing fiber action on the responsiveness of Purkinje cells to parallel fiber inputs. *Brain Res* 309: 182–186, 1984.

Ermentrout B. *Simulating, Analyzing, and Animating Dynamical Systems: A Guide to XPPAUT for Researchers and Students.* Philadelphia, PA: Society for Industrial and Applied Mathematics, 2002.

Fernandez FR, Mehaffey WH, Turner RW. Dendritic Na^+ current inactivation can increase cell excitability by delaying a somatic depolarizing afterpotential. *J Neurophysiol* 94: 3836–3848, 2005.

Genet S, Delord B. A biophysical model of nonlinear dynamics underlying plateau potentials and calcium spikes in Purkinje cell dendrites. *J Neurophysiol* 88: 2430–2444, 2002.

Hounsgaard J, Midtgaard J. Intrinsic determinants of firing pattern in Purkinje cells of the turtle cerebellum in vitro. *J Physiol* 402: 731–749, 1988.

Hounsgaard J, Midtgaard J. Synaptic control of excitability in turtle cerebellar Purkinje cells. *J Physiol* 409: 157–170, 1989.

Hsu YH, Huang HY, Tsaur ML. Contrasting expression of Kv4.3, an A-type K^+ channel, in migrating Purkinje cells and other post-migratory cerebellar neurons. *Eur J Neurosci* 18: 601–612, 2003.

Hutcheon B, Yarom Y. Resonance, oscillation and the intrinsic frequency preferences of neurons. *Trends Neurosci* 23: 216–222, 2000.

Izhikevich EM. Neural excitability, spiking, and bursting. *Int J Bifurc Chaos* 10: 1171–1266, 2000.

Izhikevich EM. *Dynamical Systems in Neuroscience: The Geometry of Excitability and Bursting.* Cambridge, MA: MIT Press, 2007.

Izhikevich EM, Desai NS, Walcott EC, Hoppensteadt FC. Bursts as a unit of neural information: selective communication via resonance. *Trends Neurosci* 26: 161–167, 2003.

Jaeger D, De Schutter E, Bower JM. The role of synaptic and voltage-gated currents in the control of Purkinje cell spiking: a modeling study. *J Neurosci* 17: 91–106, 1997.

Khaliq ZM, Gouwens NW, Raman IM. The contribution of resurgent sodium current to high-frequency firing in Purkinje neurons: an experimental and modeling study. *J Neurosci* 23: 4899–4912, 2003.

Li WC, Soffe SR, Wolf E, Roberts A. Persistent responses to brief stimuli: feedback excitation among brainstem neurons. *J Neurosci* 26: 4026–4035, 2006.

Llinas R, Sugimori M. Electrophysiological properties of in vitro Purkinje cell dendrites in mammalian cerebellar slices. *J Physiol* 305: 197–213, 1980a.

Llinas R, Sugimori M. Electrophysiological properties of in vitro Purkinje cell somata in mammalian cerebellar slices. *J Physiol* 305: 171–195, 1980b.

Loewenstein Y, Mahon S, Chadderton P, Kitamura K, Sompolinsky H, Yarom Y, Hausser M. Bistability of cerebellar Purkinje cells modulated by sensory stimulation. *Nat Neurosci* 8: 202–211, 2005.

Mainen ZF, Sejnowski TJ. Influence of dendritic structure on firing pattern in model neocortical neurons. *Nature* 382: 363–366, 1996.

Martina M, Metz AE, Bean BP. Voltage-dependent potassium currents during fast spikes of rat cerebellar Purkinje neurons: inhibition by BDS-I toxin. *J Neurophysiol* 97: 563–571, 2007.

Martina M, Yao GL, Bean BP. Properties and functional role of voltage-dependent potassium channels in dendrites of rat cerebellar Purkinje neurons. *J Neurosci* 23: 5698–5707, 2003.

McKay BE, Engbers JD, Mehaffey WH, Gordon GR, Molineux ML, Bains JS, Turner RW. Climbing fiber discharge regulates cerebellar functions by controlling the intrinsic characteristics of Purkinje cell output. *J Neurophysiol* 97: 2590–2604, 2007.

McKay BE, Molineux ML, Mehaffey WH, Turner RW. Kv1 K^+ channels control Purkinje cell output to facilitate postsynaptic rebound discharge in deep cerebellar neurons. *J Neurosci* 25: 1481–1492, 2005.

McKay BE, Turner RW. Kv3 K^+ channels enable burst output in rat cerebellar Purkinje cells. *Eur J Neurosci* 20: 729–739, 2004.

McKay BE, Turner RW. Physiological and morphological development of the rat cerebellar Purkinje cell. *J Physiol* 567: 829–850, 2005.

Montarolo PG, Palestini M, Strata P. The inhibitory effect of the olivocerebellar input on the cerebellar Purkinje cells in the rat. *J Physiol* 332: 187–202, 1982.

Pinsky PF, Rinzel J. Intrinsic and network rhythmogenesis in a reduced Traub model for CA3 neurons. *J Comput Neurosci* 1: 39–60, 1994.

Raman IM, Bean BP. Ionic currents underlying spontaneous action potentials in isolated cerebellar Purkinje neurons. *J Neurosci* 19: 1663–1674, 1999a.

Raman IM, Bean BP. Properties of sodium currents and action potential firing in isolated cerebellar Purkinje neurons. *Ann NY Acad Sci* 868: 93–96, 1999b.

Raman IM, Bean BP. Inactivation and recovery of sodium currents in cerebellar Purkinje neurons: evidence for two mechanisms. *Biophys J* 80: 729–737, 2001.

Rapp M, Segev I, Yarom Y. Physiology, morphology and detailed passive models of guinea-pig cerebellar Purkinje cells. *J Physiol* 474: 101–118, 1994.

Rinzel J. Excitation dynamics: insights from simplified membrane models. *Fed Proc* 44: 2944–2946, 1985.

Rinzel J, Ermentrout B. Analysis of neural excitability and oscillations. In: *Methods in Neuronal Modeling*, edited by Koch C, Segev I. Cambridge, MA: MIT Press, 1998, p. 251–291.

Roth A, Hausser M. Compartmental models of rat cerebellar Purkinje cells based on simultaneous somatic and dendritic patch-clamp recordings. *J Physiol* 535: 445–472, 2001.

Sacco T, Tempia F. A-type potassium currents active at subthreshold potentials in mouse cerebellar Purkinje cells. *J Physiol* 543: 505–520, 2002.

Santamaria F, Bower JM. Background synaptic activity modulates the response of a modeled Purkinje cell to paired afferent input. *J Neurophysiol* 93: 237–250, 2005.

Santamaria F, Jaeger D, De Schutter E, Bower JM. Modulatory effects of parallel fiber and molecular layer interneuron synaptic activity on Purkinje cell responses to ascending segment input: a modeling study. *J Comput Neurosci* 13: 217–235, 2002.

Schmolesky MT, Weber JT, De Zeeuw CI, Hansel C. The making of a complex spike: ionic composition and plasticity. *Ann NY Acad Sci* 978: 359–390, 2002.

Schonewille M, Khosrovani S, Winkelman BH, Hoebeek FE, De Jeu MT, Larsen IM, Van der Burg J, Schmolesky MT, Frens MA, De Zeeuw CI. Purkinje cells in awake behaving animals operate at the upstate membrane potential. *Nat Neurosci* 9: 459–461, 2006.

Seung HS, Lee DD, Reis BY, Tank DW. Stability of the memory of eye position in a recurrent network of conductance-based model neurons. *Neuron* 26: 259–271, 2000.

Stafstrom CE, Schwindt PC, Crill WE. Negative slope conductance due to a persistent subthreshold sodium current in cat neocortical neurons in vitro. *Brain Res* 236: 221–226, 1982.

Strogatz SH. *Nonlinear Dynamics and Chaos: With Applications to Physics, Biology, Chemistry, and Engineering.* Reading, MA: Addison–Wesley, 1994.

Stuart G, Hausser M. Initiation and spread of sodium action potentials in cerebellar Purkinje cells. *Neuron* 13: 703–712, 1994.

Swensen AM, Bean BP. Ionic mechanisms of burst firing in dissociated Purkinje neurons. *J Neurosci* 23: 9650–9663, 2003.

Vetter P, Roth A, Hausser M. Propagation of action potentials in dendrites depends on dendritic morphology. *J Neurophysiol* 85: 926–937, 2001.

Williams SR, Christensen SR, Stuart GJ, Hausser M. Membrane potential bistability is controlled by the hyperpolarization-activated current I(H) in rat cerebellar Purkinje neurons in vitro. *J Physiol* 539: 469–483, 2002.

Williams SR, Toth TI, Turner JP, Hughes SW, Crunelli V. The "′window" component of the low threshold Ca^{2+} current produces input signal amplification and bistability in cat and rat thalamocortical neurones. *J Physiol* 505: 689–705, 1997.

Womack M, Khodakhah K. Active contribution of dendrites to the tonic and trimodal patterns of activity in cerebellar Purkinje neurons. *J Neurosci* 22: 10603–10612, 2002.